

FUNDAMENTAL PROPERTIES OF KEPLER PLANET-CANDIDATE HOST STARS USING ASTEROSEISMOLOGY

DANIEL HUBER^{1,2}, WILLIAM J. CHAPLIN^{3,4}, JØRGEN CHRISTENSEN-DALSGAARD⁴, RONALD L. GILLILAND⁵, HANS KJELDSEN⁴, LARS A. BUCHHAVE^{6,7}, DEBRA A. FISCHER⁸, JACK J. LISSAUER¹, JASON F. ROWE¹, ROBERTO SANCHIS-OJEDA⁹, SARBANI BASU⁸, RASMUS HANDBERG⁴, SASKIA HEKKER¹⁰, ANDREW W. HOWARD¹¹, HOWARD ISAACSON¹², CHRISTOFFER KAROFF⁴, DAVID W. LATHAM¹³, MIKKEL N. LUND⁴, MIA LUNDKVIST⁴, GEOFFREY W. MARCY¹², ANDREA MIGLIO³, VICTOR SILVA AGUIRRE⁴, DENNIS STELLO^{14,4}, TORBEN ARENTOFT⁴, THOMAS BARCLAY¹, TIMOTHY R. BEDDING^{14,4}, CHRISTOPHER J. BURKE¹, JESSIE L. CHRISTIANSEN¹, YVONNE P. ELSWORTH³, MICHAEL R. HAAS¹, STEVEN D. KAWALER¹⁵, TRAVIS S. METCALFE¹⁶, FERGAL MULLALLY¹, AND SUSAN E. THOMPSON¹

accepted for publication in ApJ

ABSTRACT

We have used asteroseismology to determine fundamental properties for 66 *Kepler* planet-candidate host stars, with typical uncertainties of 3% and 7% in radius and mass, respectively. The results include new asteroseismic solutions for four host stars with confirmed planets (Kepler-4, Kepler-14, Kepler-23 and Kepler-25) and increase the total number of *Kepler* host stars with asteroseismic solutions to 77. A comparison with stellar properties in the planet-candidate catalog by Batalha et al. shows that radii for subgiants and giants obtained from spectroscopic follow-up are systematically too low by up to a factor of 1.5, while the properties for unevolved stars are in good agreement. We furthermore apply asteroseismology to confirm that a large majority of cool main-sequence hosts are indeed dwarfs and not misclassified giants. Using the revised stellar properties, we recalculate the radii for 107 planet candidates in our sample, and comment on candidates for which the radii change from a previously giant-planet/brown-dwarf/stellar regime to a sub-Jupiter size, or vice versa. A comparison of stellar densities from asteroseismology with densities derived from transit models in Batalha et al. assuming circular orbits shows significant disagreement for more than half of the sample due to systematics in the modeled impact parameters, or due to planet candidates which may be in eccentric orbits. Finally, we investigate tentative correlations between host-star masses and planet-candidate radii, orbital periods, and multiplicity, but caution that these results may be influenced by the small sample size and detection biases.

Subject headings: stars: oscillations — stars: late-type — planetary systems — techniques: photometric — techniques: spectroscopic

1. INTRODUCTION

Nearly 700 confirmed planetary systems outside our solar system have been discovered in the past two decades. The vast majority of these planets have been detected using indirect techniques such as transit photometry or Doppler velocities, which yield properties of the planet only as a function of the properties of the host star. The accurate knowledge of the fundamental properties of host stars, particularly radii and masses, is therefore of great importance for the study of extrasolar planets.

The *Kepler* Mission (Borucki et al. 2010b; Koch et al. 2010) has revolutionized exoplanet science in the last few years, yielding thousands of new exoplanet candidates (Borucki et al. 2011a,b; Batalha et al. 2013). A serious problem in the interpretation of *Kepler* planet detections, occurrence rates, and ultimately the determination of the frequency of habitable planets, is the accuracy of stellar parameters. Almost all *Kepler* planet-candidate hosts (also designated as Kepler Objects of Interest, or KOIs) are too faint to have measured parallaxes, and hence stellar parameters mostly rely on the combination of broadband photometry, stellar model atmospheres and evolutionary tracks, as done for the Kepler Input Catalog (KIC, Brown et al. 2011). Biases in the KIC have been shown to reach up to 50% in radius and 0.2 dex in $\log g$ (Verner et al. 2011b), introducing serious uncertainties in the derived planetary properties. A

¹ NASA Ames Research Center, Moffett Field, CA 94035, USA

² NASA Postdoctoral Program Fellow; daniel.huber@nasa.gov

³ School of Physics and Astronomy, University of Birmingham, Birmingham B15 2TT, UK

⁴ Stellar Astrophysics Centre, Department of Physics and Astronomy, Aarhus University, Ny Munkegade 120, DK-8000 Aarhus C, Denmark

⁵ Center for Exoplanets and Habitable Worlds, The Pennsylvania State University, 525 Davey Lab, University Park, PA 16802

⁶ Niels Bohr Institute, University of Copenhagen, DK-2100 Copenhagen, Denmark

⁷ Centre for Star and Planet Formation, Natural History Museum of Denmark, University of Copenhagen, DK-1350 Copenhagen, Denmark

⁸ Department of Astronomy, Yale University, New Haven, CT 06511, USA

⁹ Department of Physics, Massachusetts Institute of Technology, 77 Massachusetts Ave., Cambridge, MA 02139, USA

¹⁰ Astronomical Institute 'Anton Pannekoek', University of Amsterdam, Science Park 904, 1098 XH Amsterdam, The Netherlands

¹¹ Institute for Astronomy, University of Hawaii, 2680 Woodlawn Drive, Honolulu, HI 96822, USA

¹² Department of Astronomy, University of California, Berkeley, California 94720, USA

¹³ Harvard-Smithsonian Center for Astrophysics, 60 Garden Street, Cambridge, Massachusetts 02138, USA

¹⁴ Sydney Institute for Astronomy (SfA), School of Physics, University of Sydney, NSW 2006, Australia

¹⁵ Department of Physics and Astronomy, Iowa State University, Ames, IA 50011 USA

¹⁶ Space Science Institute, Boulder, CO 80301, USA

more favorable case are hosts for which high-resolution spectroscopy is available, which yields strong constraints on the evolutionary state. Recent spectroscopic efforts on planet-candidate hosts have concentrated on cool M-dwarfs (Johnson et al. 2012; Muirhead et al. 2012a,b) as well as F-K dwarfs (Buchhave et al. 2012). Nevertheless, spectroscopic analyses are often affected by degeneracies between T_{eff} , $\log g$ and $[\text{Fe}/\text{H}]$ (Torres et al. 2012), and only yield strongly model-dependent constraints on stellar radius and mass.

An excellent alternative to derive accurate stellar radii and masses of host stars is asteroseismology, the study of stellar oscillations (see, e.g., Brown & Gilliland 1994; Christensen-Dalsgaard 2004; Aerts et al. 2010; Gilliland et al. 2010b). Prior to the *Kepler* mission, asteroseismology of exoplanet hosts was restricted to a few stars with detections from ground-based Doppler observations (Bouchy et al. 2005; Vauclair et al. 2008; Wright et al. 2011) or the Hubble space telescope (Gilliland et al. 2011; Nutzman et al. 2011). This situation has dramatically changed with the launch of the *Kepler* space telescope, which provides photometric data suitable for both transit searches and asteroseismology. First results for previously-known transiting planet hosts in the *Kepler* field were presented by Christensen-Dalsgaard et al. (2010), and several *Kepler* planet discoveries have since benefitted from asteroseismic constraints of host-star properties (Batalha et al. 2011; Howell et al. 2012; Barclay et al. 2012; Borucki et al. 2012; Carter et al. 2012; Chaplin et al. 2013; Barclay et al. 2013; Gilliland et al. 2013). In this paper, we present the first systematic study of *Kepler* planet-candidate host stars using asteroseismology.

2. DETERMINATION OF FUNDAMENTAL STELLAR PROPERTIES

2.1. Background

Solar-like oscillations are acoustic standing waves excited by near-surface convection (see, e.g., Houdek et al. 1999; Houdek 2006; Samadi et al. 2007). The oscillation modes are characterized by a spherical degree l (the total number of surface nodal lines), a radial order n (the number of nodes from the surface to the center of the star) and an azimuthal order m (the number of surface nodal lines that cross the equator). The azimuthal order m is generally only important if the $(2l + 1)$ degeneracy of frequencies of degree l is lifted by rotation.

Solar-like oscillations involve modes of low spherical degree l and high radial order n , and hence the frequencies can be asymptotically described by a series of characteristic separations (Vandakurov 1968; Tassoul 1980; Gough 1986). The large frequency separation $\Delta\nu$ is the spacing between modes with the same spherical degree l and consecutive radial order n , and probes the sound travel time across the stellar diameter. This means that $\Delta\nu$ is related to the mean stellar density and is expected to scale as follows (Ulrich 1986):

$$\Delta\nu = \frac{(M/M_{\odot})^{1/2}}{(R/R_{\odot})^{3/2}} \Delta\nu_{\odot}. \quad (1)$$

Another fundamental observable is the frequency at which the oscillations have maximum power (ν_{max}). As

first argued by Brown et al. (1991), ν_{max} for sun-like stars is expected to scale with the acoustic cut-off frequency and can therefore be related to fundamental stellar properties, as follows (Kjeldsen & Bedding 1995):

$$\nu_{\text{max}} = \frac{M/M_{\odot}}{(R/R_{\odot})^2 \sqrt{T_{\text{eff}}/T_{\text{eff},\odot}}} \nu_{\text{max},\odot}. \quad (2)$$

Equation (2) shows that ν_{max} is mainly dependent on surface gravity, and hence is a good indicator of the evolutionary state. Typical oscillation frequencies range from $\sim 3000 \mu\text{Hz}$ for main sequence stars like our Sun down to $\sim 300 \mu\text{Hz}$ for low-luminosity red giants, and a few μHz for high-luminosity giants. We note that while individual oscillation frequencies provide more detailed constraints on properties such as stellar ages (see, e.g., Doğan et al. 2010; Metcalfe et al. 2010; di Mauro et al. 2011; Mathur et al. 2012; Metcalfe et al. 2012), the extraction of frequencies is generally only possible for high S/N detections. To extend our study to a large ensemble of planet-candidate hosts, we therefore concentrate solely on determining the global oscillation properties $\Delta\nu$ and ν_{max} in this paper.

It is important to note that Equations (1) and (2) are approximate relations which require calibration. For comprehensive reviews of theoretical and empirical tests of both relations we refer the reader to Belkacem (2012) and Miglio et al. (2013a), but we provide a brief summary here. It is well known that Equation (2) is on less firm ground than Equation (1) due to uncertainties in modeling convection which drives the oscillations, although recent progress on the theoretical understanding of Equation (2) has been made (Belkacem et al. 2011). Stello et al. (2009) showed that both relations agree with models to a few percent, which was supported by investigating the relation between $\Delta\nu$ and ν_{max} for a large ensemble of *Kepler* and CoRoT stars, and by comparing derived radii and masses to evolutionary tracks and synthetic stellar populations (Hekker et al. 2009; Miglio et al. 2009; Kallinger et al. 2010a; Huber et al. 2010; Mosser et al. 2010; Huber et al. 2011; Silva Aguirre et al. 2011; Miglio et al. 2012a). More recently, White et al. (2011) showed that that $\Delta\nu$ calculated from individual model frequencies can systematically differ from $\Delta\nu$ calculated using Equation (1) by up to 2% for giants and for dwarfs with $M/M_{\odot} \gtrsim 1.2$. Similar results were found by Mosser et al. (2013), who investigated the influence of correcting the observed $\Delta\nu$ to the value expected in the high-frequency asymptotic limit. In general, however, comparisons with individual frequency modeling have shown agreement within 2% and 5% in radius and mass, respectively, both for dwarfs (Mathur et al. 2012) and for giants (di Mauro et al. 2011; Jiang et al. 2011).

Empirical tests have been performed using independently determined fundamental properties from Hipparcos parallaxes, eclipsing binaries, cluster stars, and optical long-baseline interferometry (see, e.g., Stello et al. 2008; Bedding 2011; Brogaard et al. 2012; Miglio 2012; Miglio et al. 2012b; Huber et al. 2012; Silva Aguirre et al. 2012). For unevolved stars ($\log g \gtrsim 3.8$) no evidence for systematic deviations has yet been determined within the observational uncertainties, with upper limits of $\lesssim 4\%$ in radius (Huber et al. 2012) and

$\lesssim 10\%$ in mass (Miglio 2012). For giants and evolved subgiants ($\log g \lesssim 3.8$) similar results have been reported, although a systematic deviation of $\sim 3\%$ in $\Delta\nu$ has recently been noted for He-core burning red giants (Miglio et al. 2012b).

In summary, for stars considered in this study, Equations (1) and (2) have been tested theoretically to $\sim 2\%$ and $\sim 5\%$, as well as empirically to $\lesssim 4\%$ and $\lesssim 10\%$ in radius and mass, respectively. While it should be kept in mind that future revisions of these relations based on more precise empirical data are possible, it is clear that these uncertainties are significantly smaller than for classical methods to determine radii and masses of field stars.

2.2. Asteroseismic Analysis

Our analysis is based on *Kepler* short-cadence (Gilliland et al. 2010a) and long-cadence (Jenkins et al. 2010) data through Q11. We have used simple-aperture photometry (SAP) data for our analysis. We have analyzed all available data for the 1797 planet-candidate hosts listed in the cumulative catalog by Batalha et al. (2013). Before searching for oscillations, transits need to be removed or corrected since the sharp structure in the time domain would cause significant power leakage from low frequencies into the oscillation frequency domain. This was done using a median filter with a length chosen according to the measured duration of the transit. In an alternative approach, all transits were phase-clipped from the time series using the periods and epochs listed in Batalha et al. (2013). Note that for typical transit durations and periods, the induced gaps in the time series have little influence on the resulting power spectrum. Finally, all time series were high-pass filtered by applying a quadratic Savitzky-Golay filter (Savitzky & Golay 1964) to remove additional low-frequency power due to stellar activity and instrumental variability. For short-cadence data, the typical cut-off frequency was $\sim 100 \mu\text{Hz}$, while for long-cadence data a cut-off of $\sim 1 \mu\text{Hz}$ was applied.

To detect oscillations and extract the global oscillation parameters $\Delta\nu$ and ν_{max} , we have used the analysis pipelines described by Huber et al. (2009), Hekker et al. (2010), Karoff et al. (2010), Verner & Roxburgh (2011) and Lund et al. (2012). Note that these methods have been extensively tested on *Kepler* data and were shown to agree well with other methods (Hekker et al. 2011b; Verner et al. 2011a; Hekker et al. 2012). We successfully detect oscillations in a total of 77 planet-candidate hosts (including 11 stars for which asteroseismic solutions have been published in separate studies). For 69 host stars short-cadence data were used, while 8 of them showed oscillations with ν_{max} values low enough to allow a detection using long-cadence data. The final values for $\Delta\nu$ and ν_{max} are listed in Table 1 and were adopted from the method of Huber et al. (2009), with uncertainties calculated by adding in quadrature the formal uncertainty and the scatter of the values over all other methods. Note that in some cases the S/N was too low to reliably estimate ν_{max} , and hence only $\Delta\nu$ is listed. For one host (KOI-1054) $\Delta\nu$ could not be reliably determined, and hence only ν_{max} is listed. The solar reference values, which were calculated using the same method, are $\Delta\nu_{\odot} = 135.1 \pm 0.1 \mu\text{Hz}$ and $\nu_{\text{max},\odot} = 3090 \pm 30 \mu\text{Hz}$ (Huber et al. 2011).

We note that in the highest S/N cases, the observa-

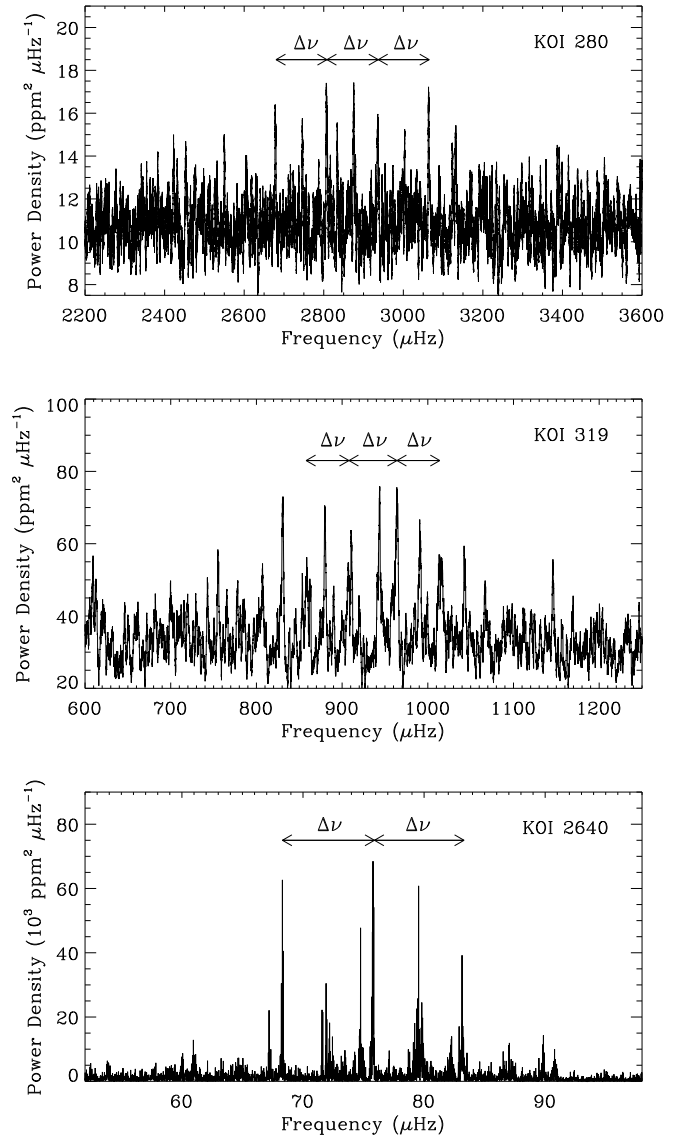


FIG. 1.— Power spectra for three *Kepler* planet-candidate host stars with detected solar-like oscillations. The panels show three representative hosts in different evolutionary stages: a main-sequence star (top panel), a subgiant (middle panel) and a red giant (bottom panel). For the latter long-cadence data were used, while the former two have been calculated using short-cadence data. The large frequency separation $\Delta\nu$ is indicated in each panel. Note the increase in the y-axis scale from the top to bottom panel, illustrating the increase in oscillation amplitudes for evolved stars.

tional uncertainties on $\Delta\nu$ are comparable to or lower than the accuracy to which Equation (1) has been tested (see previous section). To account for systematic errors in Equation (1), we adopt a conservative approach by adding to our uncertainties in quadrature the difference between the observed $\Delta\nu$ and the corrected $\Delta\nu$ using Equation (5) in White et al. (2011). To account for the fact that $\Delta\nu$ can be measured more precisely than ν_{max} , the same fractional uncertainties were added in quadrature to the formal ν_{max} uncertainties. The final median uncertainties in $\Delta\nu$ and ν_{max} are 2% and 4%, respectively.

Figure 1 shows examples of power spectra for three stars in the sample, illustrating a main-sequence star (top

panel), a subgiant (middle panel) and a red-giant (bottom panel). Note that the power spectra illustrate typical intermediate S/N detections. Broadly speaking the detectability of oscillations depends on the brightness of the host star and the evolutionary state, because oscillation amplitudes scale proportionally to stellar luminosity (see, e.g., Kjeldsen & Bedding 1995; Chaplin et al. 2011b). Among host stars that are close to the main-sequence ($\log g > 4.2$), the faintest star with detected oscillations has a *Kepler* magnitude of 12.4 mag.

2.3. Spectroscopic Analysis

In addition to asteroseismic constraints, effective temperatures and metallicities are required to derive a full set of fundamental properties. For all stars in our sample high-resolution optical spectra were obtained as part of the *Kepler* follow-up program (Gautier et al. 2010). Spectroscopic observations were taken using four different instruments: the HIRES spectrograph (Vogt et al. 1994) on the 10-m telescope at Keck Observatory (Mauna Kea, Hawaii), the FIES spectrograph (Djupvik & Andersen 2010) on the 2.5-m Nordic Optical Telescope at the Roque de los Muchachos Observatory (La Palma, Spain), the TRES spectrograph (Fürész 2008) on the 1.5-m Tillinghast reflector at the F. L. Whipple Observatory (Mt. Hopkins, Arizona), and the Tull Coudé spectrograph on the 2.7-m Harlan J. Smith Telescope at McDonald Observatory (Fort Davis, Texas). Typical resolutions of the spectra range from 40,000–70,000. Atmospheric parameters were derived using either the Stellar Parameter Classification (SPC, see Buchhave et al. 2012) or Spectroscopy Made Easy (SME, see Valenti & Piskunov 1996) pipelines. Both methods match the observed spectrum to synthetic model spectra in the optical wavelengths and yield estimates of T_{eff} , $\log g$, metallicity and $v \sin(i)$. Note that in our analysis we have assumed that the metal abundance $[m/H]$, as returned by SPC, is equivalent to the iron abundance $[\text{Fe}/H]$. For stars with multiple observations each spectrum was analyzed individually, and the final parameters were calculated as an average of the individual results weighted by the cross-correlation function (CCF), which gives a measure of the quality of the fit compared to the spectral template. To ensure a homogenous set of parameters, we adopt the spectroscopic values from SPC, which was used to analyze the entire sample of host stars. Table 1 lists for each planet-candidate host the details of the SPC analysis such as the number of spectra used, the average S/N of the observations, the average CCF, and the instrument used to obtain the spectra.

As discussed by Torres et al. (2012), spectroscopic methods such as SME and SPC suffer from degeneracies between T_{eff} , $\log g$ and $[\text{Fe}/H]$. Given the weak dependency of ν_{max} on T_{eff} (see Equation (2)), asteroseismology can be used to remove such degeneracies by fixing $\log g$ in the spectroscopic analysis to the asteroseismic value (see, e.g., Bruntt et al. 2012; Morel & Miglio 2012; Thygesen et al. 2012). This is done by performing the asteroseismic analysis (see next section) using initial estimates of T_{eff} and $[\text{Fe}/H]$ from spectroscopy, and iterating both analyses until convergence is reached (usually after one iteration). We have applied this method to all host stars in our sample to derive asteroseismically constrained values of T_{eff} and $[\text{Fe}/H]$, which are

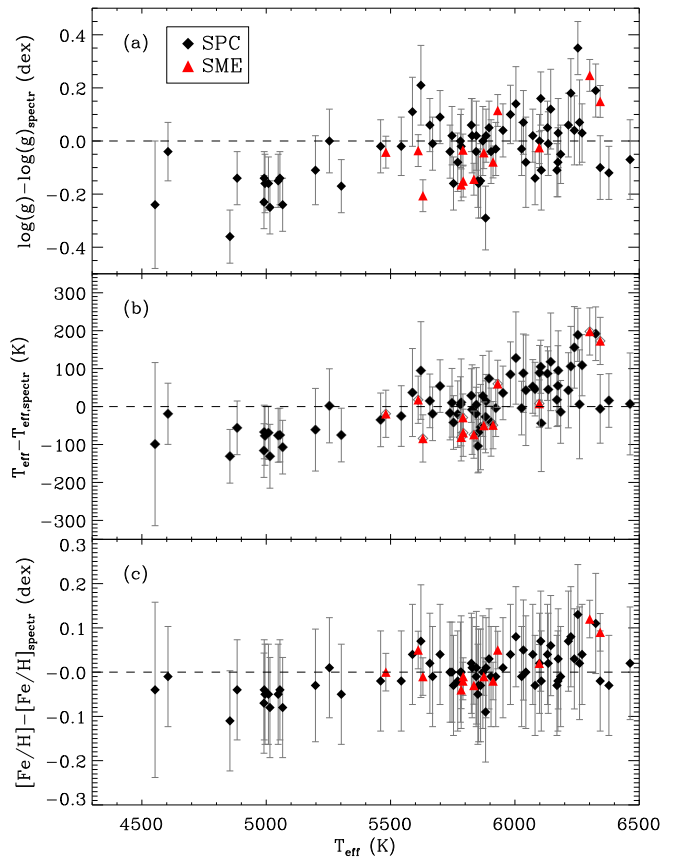


FIG. 2.— (a) Comparison of $\log g$ from a spectroscopic analysis with and without asteroseismic constraints on $\log g$. The difference is shown in the sense of constrained minus unconstrained analysis. Black diamonds show the sample analyzed with SPC, and red triangles stars analyzed with SME. (b) Same as panel (a) but for T_{eff} . (c) Same as panel (a) but for $[\text{Fe}/H]$.

listed in Table 2. Note that since SPC has been less tested for giants, we have adopted more conservative error bars of 80 K in T_{eff} and 0.15 dex in $[\text{Fe}/H]$ for all evolved giants with $\log g < 3$ (Thygesen et al. 2012). For all stars in our sample, we have added contributions of 59 K in T_{eff} and 0.062 dex in $[\text{Fe}/H]$ in quadrature to the formal uncertainties to account for systematic differences between spectroscopic methods, as suggested by Torres et al. (2012).

Our sample allows us to investigate the effects of fixing $\log g$ on the determination of T_{eff} and $[\text{Fe}/H]$. This is analogous to the work of Torres et al. (2012), who used stellar densities derived from transits to independently determine $\log g$ for a sample of main-sequence stars. Figure 2 shows the differences in $\log g$, T_{eff} and $[\text{Fe}/H]$ as a function of T_{eff} . As in the Torres et al. (2012) sample, the unconstrained analysis tends to slightly underestimate $\log g$ (and hence T_{eff} and $[\text{Fe}/H]$) for stars hotter than ~ 6000 K. More serious systematics are found for stars with $T_{\text{eff}} \lesssim 5400$ K, which in our sample corresponds to subgiant and giant stars, for which $\log g$ is systematically overestimated by up to 0.2 dex. The effect of these systematics on planet-candidate radii will be discussed in detail in Section 3.1.

Figure 2 shows that changes in $\log g$ are correlated with changes in T_{eff} and $[\text{Fe}/H]$. We have investigated the partial derivatives $\Delta T_{\text{eff}}/\Delta \log g$ and $\Delta [\text{Fe}/H]/\Delta \log g$

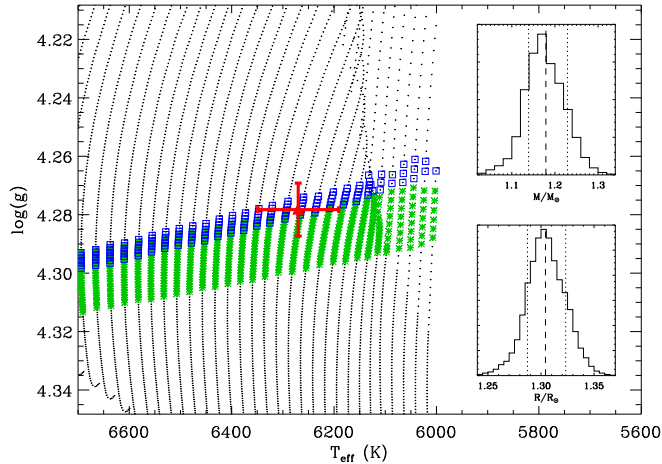


FIG. 3.— Surface gravity versus T_{eff} for BaSTI evolutionary tracks with a metallicity of $[\text{Fe}/\text{H}] = +0.02$ in steps of $0.01M_{\odot}$. Colored symbols show the $\pm 1\sigma$ constraints from ν_{max} (green asterisks) and $\Delta\nu$ (blue squares) for KOI-244 (Kepler-25). The determined position is shown as a red diamond. The inset illustrates the distributions of Monte-Carlo simulations for stellar mass and radius, with dashed and dotted lines corresponding to the median and $\pm 1\sigma$ confidence limits, respectively.

and did not find a significant dependence on stellar properties such as effective temperature. The median derivatives for our sample are $\Delta T_{\text{eff}}/\Delta \log g = 475 \pm 60 \text{ K/dex}$ and $\Delta[\text{Fe}/\text{H}]/\Delta \log g = 0.31 \pm 0.03$, respectively. Hence, a change of $\log g = 0.1 \text{ dex}$ typically corresponds to a change of $\sim 50 \text{ K}$ in T_{eff} and 0.03 dex in $[\text{Fe}/\text{H}]$.

The results in this study can also be used to test temperatures based on broadband photometry. A comparison of 46 dwarfs which overlap with the sample of Pinsonneault et al. (2012) showed that the photometric temperatures (corrected for the spectroscopic metallicities in Table 2) are on average 190 K hotter than our spectroscopic estimates, with a scatter of 130 K. This offset is larger than previous comparisons based on a brighter comparison sample (see Pinsonneault et al. 2012), pointing to a potential problem with interstellar reddening. The results of our study, combined with other samples for which both asteroseismology and spectroscopy are available (Molenda-Żakowicz et al. 2011; Bruntt et al. 2012; Thygesen et al. 2012), will be a valuable calibration sample to improve effective temperatures in the *Kepler* field based on photometric techniques such as the infrared flux method (Casagrande et al. 2010).

2.4. Grid-Modelling

Given an estimate of the effective temperature, Equations (1) and (2) can be used to calculate the mass and radius of a star (see, e.g., Kallinger et al. 2010b). However, since both equations allow radius and temperature to vary freely for any given mass, a more refined method is to include knowledge from evolutionary theory to match the spectroscopic parameters with asteroseismic constraints. This so-called grid-based method has been used extensively both for unevolved and evolved stars (Stello et al. 2009; Kallinger et al. 2010a; Chaplin et al. 2011a; Creevey et al. 2012; Basu et al. 2010, 2012).

To apply the grid-based method, we have used different model tracks: the Aarhus Stellar Evolution Code (ASTEC, Christensen-Dalsgaard 2008), the Bag

of Stellar Isochrones (BaSTI, Pietrinferni et al. 2004), the Dartmouth Stellar Evolution Database (DSEP, Dotter et al. 2008), the Padova stellar evolution code (Marigo et al. 2008), the Yonsei-Yale isochrones (YY, Demarque et al. 2004), and the Yale Rotating Stellar Evolution Code (YREC, Demarque et al. 2008). To derive masses and radii we have employed several different methods (da Silva et al. 2006; Stello et al. 2009; Basu et al. 2011; Miglio et al. 2013b; Silva Aguirre et al. 2013). In brief, the methods calculate a likelihood function for a set of independent Gaussian observables X :

$$\mathcal{L}_X = \frac{1}{\sqrt{2\pi}\sigma_X} \exp\left(-\frac{(X_{\text{obs}} - X_{\text{model}})^2}{2\sigma_X^2}\right) \quad (3)$$

with $X = \{T_{\text{eff}}, [\text{Fe}/\text{H}], \nu_{\text{max}}, \Delta\nu\}$. The combined likelihood is:

$$\mathcal{L} = \mathcal{L}_{T_{\text{eff}}} \mathcal{L}_{[\text{Fe}/\text{H}]} \mathcal{L}_{\nu_{\text{max}}} \mathcal{L}_{\Delta\nu}. \quad (4)$$

Note that for cases where only $\Delta\nu$ could be measured, the ν_{max} term in Equation (4) was omitted. The best-fitting model is then identified from the likelihood distribution for a given physical parameter, e.g. stellar mass and radius. Uncertainties are calculated, for example, by performing Monte-Carlo simulations using randomly drawn values for the observed values of T_{eff} , $[\text{Fe}/\text{H}]$, ν_{max} and $\Delta\nu$. For an extensive comparison of these methods, including a discussion of potential systematics, we refer the reader to Gai et al. (2011).

As an example, Figure 3 shows a diagram of $\log g$ versus T_{eff} for KOI-244 (Kepler-25), with evolutionary tracks taken from the BaSTI grid. The blue and green areas show models within $1\text{-}\sigma$ of the observationally measured values of $\Delta\nu$ and ν_{max} , respectively. The insets show histograms of Monte-Carlo simulations for mass and radius. The best-fitting values were calculated as the median and 84.1 and 15.9 percentile (corresponding to the 1σ confidence limits) of the distributions.

To account for systematics due to different model grids, the final parameters for each star were calculated as the median over all methods, with uncertainties estimated by adding in quadrature the median formal uncertainty and the scatter over all methods. Table 2 lists the final parameters for all host stars in our sample. The median uncertainties in radius and mass are 3% and 7%, respectively, consistent with the limits discussed in Section 2.1. Note that for 11 hosts we have adopted the solutions published in separate papers. We also note that for some stars the mass and radius distributions are not symmetric due to the ‘‘hook’’ in evolutionary tracks just before Hydrogen exhaustion in the core (see Figure 3). In general, however, variations in the results of different model grids are larger than these asymmetries and hence it is valid to assume symmetric (Gaussian) error bars, as reported in Table 2. Table 2 also reports the stellar density directly derived from Equation (1). Importantly, the stellar properties presented here are independent of the properties of the planets themselves, and hence can be directly used to re-derive planetary parameters. Table 3 lists revised radii and semi-major axes for the 107 planet candidates in our sample, calculated using the transit parameters in Batalha et al. (2013).

To check the consistency of the stellar properties, we

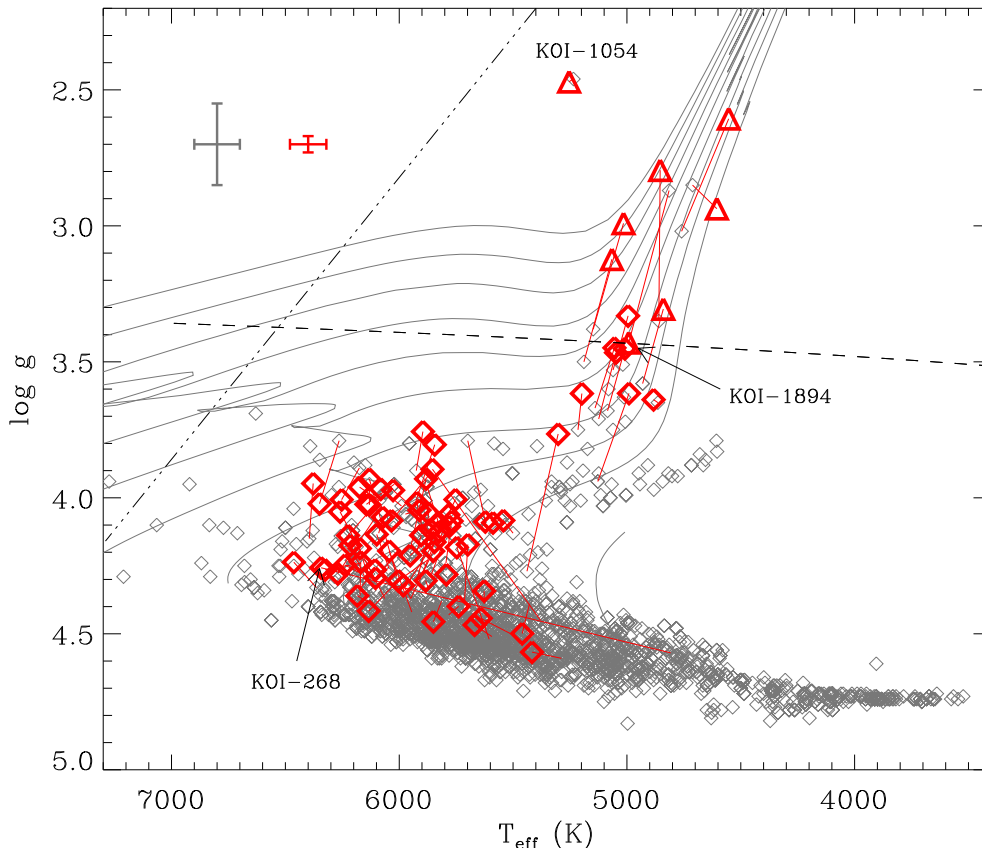


FIG. 4.— Surface gravity versus effective temperature for planet-candidate hosts in the Batalha et al. (2013) catalog (grey diamonds), together with solar metallicity Yonsei-Yale evolutionary tracks from $0.8\text{--}2.6 M_{\odot}$ in steps of $0.2 M_{\odot}$ (grey lines). The dashed-dotted line marks the approximate location of the cool edge of the instability strip, and the dashed line marks the long-cadence Nyquist limit. Thick red symbols show the revised positions of 77 host stars with asteroseismic detections using long-cadence (triangles) and short-cadence (diamonds) data, respectively. Thin red lines connect the revised positions to the values in Batalha et al. (2013). Typical error bars for stars with spectroscopic follow-up only (grey) and with asteroseismic constraints (red) are shown in the top left side of the plot. A few host stars that are discussed in more detail in the text are annotated.

compared the final radius and mass estimates in Table 2 with those calculated by solving Equations (1) and (2) (the direct method) for stars which have both reliable ν_{\max} and $\Delta\nu$ measurements. We found excellent agreement between both determinations, with no systematic deviations and a scatter consistent with the uncertainties from the direct method.

3. COMPARISON WITH PREVIOUS STELLAR PARAMETERS

3.1. Revised stellar parameters in Batalha et al. (2013)

The planet-candidate catalog by Batalha et al. (2013) included a revision of stellar properties based on matching available constraints to Yonsei-Yale evolutionary tracks. This revision (hereafter referred to as YY values) was justified since KIC surface gravities for some stars, in particular for cool M-dwarfs and for G-type dwarfs, seemed unphysical compared to predictions from stellar evolutionary theory. When available, the starting values for this revision were spectroscopic solutions, while for the remaining stars KIC parameters were used as initial guesses. Our derived stellar parameters allow us to test this revision based on our subset of planet-candidate hosts.

Figure 4 shows surface gravity versus effective temperature for all planet-candidate hosts in the Batalha et al.

(2013) catalog. The nearly horizontal dashed line shows the long-cadence Nyquist limit, below which short-cadence data are needed to sufficiently sample the oscillations. Thick red symbols in the plot show all host stars for which we have detected oscillations using short-cadence data (diamonds) and long-cadence data (triangles). Note that the T_{eff} and $\log g$ values plotted for these stars were derived from the combination of asteroseismology and spectroscopy, as discussed in Section 2 (see also Table 2). For each detection, a thin line connects the position of the star determined in this work to the values published in Batalha et al. (2013).

Figure 4 shows that our sample consists primarily of slightly evolved F to G-type stars. This is due to the larger oscillation amplitudes in these stars compared to their unevolved counterparts. We observe no obvious systematic shift in $\log g$ for unevolved stars, while surface gravities for evolved giants and subgiants were generally overestimated compared to the asteroseismic values. To illustrate this further, Figure 5 shows the difference between fundamental properties ($\log g$, radius, mass and temperature) from the asteroseismic analysis and the values given by Batalha et al. (2013) as a function of surface gravity. Red triangles mark stars for which KIC parameters were used as initial values, while black diamonds are stars for which spectroscopic solutions were used. In the

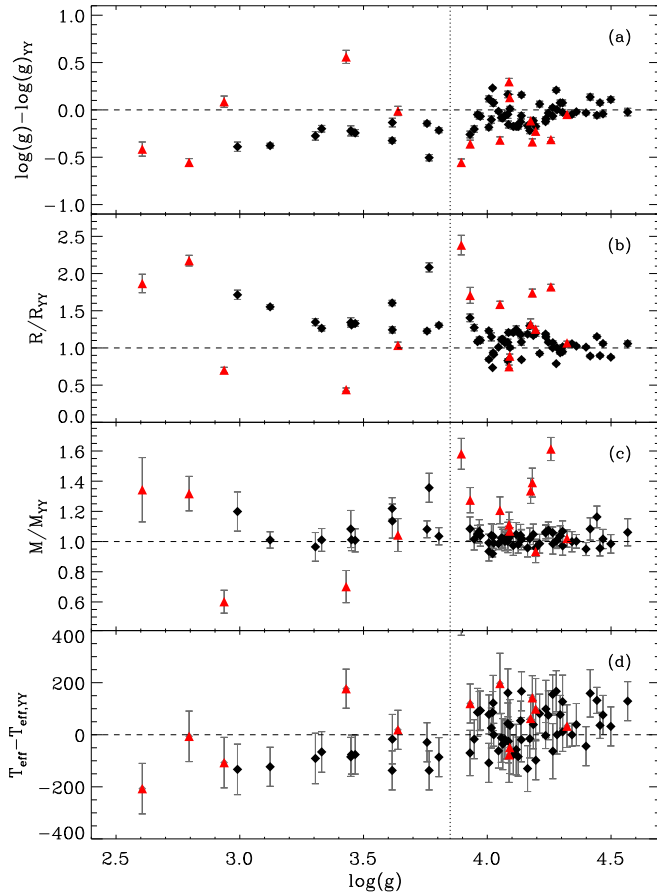


FIG. 5.— (a) Difference between $\log g$ determined from asteroseismology and $\log g$ given in Batalha et al. (2013) as a function of seismic $\log g$ for all host stars in our sample. Red triangles mark stars for which the revised parameters in Batalha et al. (2013) are based on KIC parameters, while black diamonds are stars for which spectroscopic solutions were used. The vertical dotted line divides evolved stars ($\log g < 3.85$) from unevolved stars ($\log g > 3.85$). (b) Same as panel (a) but for stellar radii. (c) Same as panel (a) but for stellar masses. (d) Same as panel (a) but for stellar effective temperatures. Note that KOI-1054 has been omitted from this figure since no full set of stellar properties was derived (see text).

following we distinguish between unevolved and evolved stars using a cut at $\log g = 3.85$ (see dotted line in Figure 5), which roughly divides our sample between stars before and after they reached the red-giant branch.

Table 4 summarizes the mean differences between values derived in this work and the values given by Batalha et al. (2013). If we only use unevolved stars ($\log g > 3.85$), the differences for stars with spectroscopic follow-up (black diamonds in Figure 5) are small, with an average difference of -0.04 ± 0.02 dex (scatter of 0.12 dex) in $\log g$ and $6 \pm 2\%$ (scatter of 15%) in radius. For stars based on KIC parameters (red triangles in Figure 5), the mean differences are considerably larger with -0.17 ± 0.10 dex (scatter of 0.29 dex) in $\log g$ and $41 \pm 17\%$ (scatter of 52%) in radius. This confirms previous studies predicting overestimated KIC radii for *Kepler* targets (Verner et al. 2011b; Gaidos & Mann 2013) and shows that, as expected, spectroscopy yields a strong improvement (both in reduced scatter and offset) compared to the KIC. This emphasizes the need for a systematic spectroscopic follow-up of all planet-candidate hosts.

The unevolved planet-candidate host with the largest change in stellar parameters from this study is KOI-268 (see annotation in Figure 4), which has previously been classified as a late K-dwarf with $T_{\text{eff}} \sim 4800$ K, hosting a $1.6 R_{\oplus}$ planet in a 110 d orbit. Our asteroseismic analysis yields $\log g = 4.26 \pm 0.01$, which is clearly incompatible with a late-type dwarf. Follow-up spectroscopy revised T_{eff} for this star to 6300 K, correctly identifying it as a F-type dwarf. The revised radius for the planet candidate based on the stellar parameters presented here is $3.00 \pm 0.06 R_{\oplus}$ (compared to the previous estimate of $1.6 R_{\oplus}$).

We note that four unevolved hosts in our sample are confirmed planetary systems that until now had no available asteroseismic constraints: Kepler-4 (Borucki et al. 2010a), Kepler-14 (Buchhave et al. 2011), Kepler-23 (Ford et al. 2012) and Kepler-25 (Steffen et al. 2012b). The agreement with the host-star properties published in the discovery papers (based on spectroscopic constraints with evolutionary tracks) is good, and the stellar parameters presented here will be valuable for future studies of these systems. We have also compared our results for Kepler-4 and Kepler-14 with stellar properties published by Southworth (2011) and Southworth (2012), and found good agreement within $1 - \sigma$ for mass and radius.

Turning to evolved hosts ($\log g < 3.85$), the differences between the asteroseismic and YY values for stars with spectroscopic follow-up (black diamonds in Figure 5) are on average -0.27 ± 0.03 dex (scatter of 0.11 dex) in $\log g$ and $44 \pm 5\%$ (scatter of 17%) in radius. For stars based on KIC parameters (red triangles in Figure 5), the mean differences are -0.1 ± 0.2 dex (scatter of 0.5 dex) in $\log g$ and $24 \pm 37\%$ (scatter of 83%) in radius. Unlike for unevolved stars, the parameters based on spectroscopy are systematically overestimated in $\log g$, and hence yield planet-candidate radii that are systematically underestimated by up to a factor of 1.5. This bias is not present in the YY properties based on initial values in the KIC (although the scatter is high), and illustrates the importance of coupling asteroseismic constraints with spectroscopy, particularly for evolved stars.

Figure 6 shows planet-candidate radii versus orbital periods for the full planet-candidate catalog, highlighting all candidates in our sample with revised radii $< 50 R_{\oplus}$ in red. As in Figure 4, thin lines connect our red-derived radii to the values published by Batalha et al. (2013). For a few evolved host stars, the revised host radii change the status of the candidates from planetary companions to objects that are more compatible with brown dwarfs or low-mass stars. The first planet-candidate host that was identified as a false-positive using asteroseismology was KOI-145.01, as discussed by Gilliland et al. (2010b). KOI-2640.01 is another example for a potential asteroseismically determined false-positive, with an increase of the companion radius from $9 R_{\oplus}$ to $17.0 \pm 0.8 R_{\oplus}$. Additionally, the companions of KOI-1230 and KOI-2481 are now firmly placed in the stellar mass regime with revised radii of $64 \pm 2 R_{\oplus}$ ($0.58 \pm 0.02 R_{\odot}$) and $31 \pm 2 R_{\oplus}$ ($0.29 \pm 0.02 R_{\odot}$), respectively. On the other hand, for KOI-1894 the companion radius becomes sufficiently small to qualify the companion as a sub-Jupiter size planet candidate, with a decreased radius from $16.3 R_{\oplus}$ to $7.2 \pm 0.4 R_{\oplus}$. KOI-1054 is a peculiar star in the sample with a very low metallicity ($[\text{Fe}/\text{H}] = -0.9$ dex). Despite the lack of a reliable

TABLE 4
MEAN DIFFERENCES BETWEEN HOST-STAR PROPERTIES IN THIS STUDY AND AS GIVEN IN BATALHA ET AL. (2013).

Parameter	$\log g > 3.85$		$\log g < 3.85$	
	Spectroscopy	KIC	Spectroscopy	KIC
$\Delta(\log g)$ (dex)	-0.04 ± 0.02 (0.12)	-0.17 ± 0.10 (0.29)	-0.27 ± 0.03 (0.11)	-0.1 ± 0.2 (0.5)
$\Delta(R)$ (%)	6 ± 2 (15)	41 ± 17 (52)	44 ± 5 (17)	24 ± 37 (83)
$\Delta(M)$ (%)	2 ± 1 (4)	21 ± 7 (21)	9 ± 3 (11)	1 ± 16 (36)
$\Delta(T_{\text{eff}})$ (K)	31 ± 12 (84)	111 ± 47 (141)	-88 ± 12 (42)	-25 ± 70 (155)

Differences are given in the sense of values derived in this work minus the values given in Batalha et al. (2013). Error bars are the standard error of the mean, and numbers in brackets are the standard deviation of the residuals.

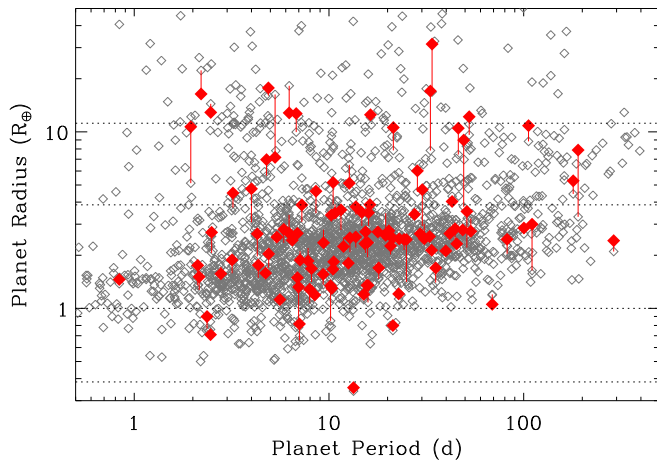


FIG. 6.— Planet radius versus orbital period for all candidates in the catalog by Batalha et al. (2013). Thick red diamonds show the rederived radii for all planetary candidates included in our sample with revised radii $< 50R_{\oplus}$, with thin red lines connecting the updated radii to those published in the *Kepler* planet-candidate catalog (Batalha et al. 2013). Dotted lines mark the radii of Mercury, Earth, Neptune and Jupiter.

$\Delta\nu$ measurement our study confirms that this star is an evolved giant with $\log g = 2.47 \pm 0.01$ dex, indicating that the potential companion with an orbital period of only 3.3 days is likely a false-positive.

3.2. Identification of misclassified Giants

A recent study by Mann et al. (2012) showed that $\sim 96\%$ of all bright ($K_p < 14$) and cool ($T_{\text{eff}} < 4500$ K) stars in the *Kepler* Input Catalog are giants. This raises considerable worry about a giant contamination among the cool planet-candidate host sample, and has implications for studies of planet detection completeness and the occurrence rates of planets with a given size. Asteroseismology provides an efficient tool to identify giants using *Kepler* photometry alone, without the need for follow-up observations. Since oscillation amplitudes scale with stellar luminosity (see, e.g., the y-axis scale in Figure 1), giants show large amplitudes that are detectable in all typical *Kepler* targets. In addition, oscillation timescales scale with stellar luminosity, with frequencies for red giants falling well below the long-cadence Nyquist limit (see, e.g., Bedding et al. 2010; Hekker et al. 2011a; Mosser et al. 2012). Hence, any cool giant should show detectable oscillations using long-cadence data, which is readily available for all *Kepler* targets.

A few caveats to this method exist. First, there is a cut-off in temperature below which the variability is too slow to reliably measure oscillations. For data up to Q11

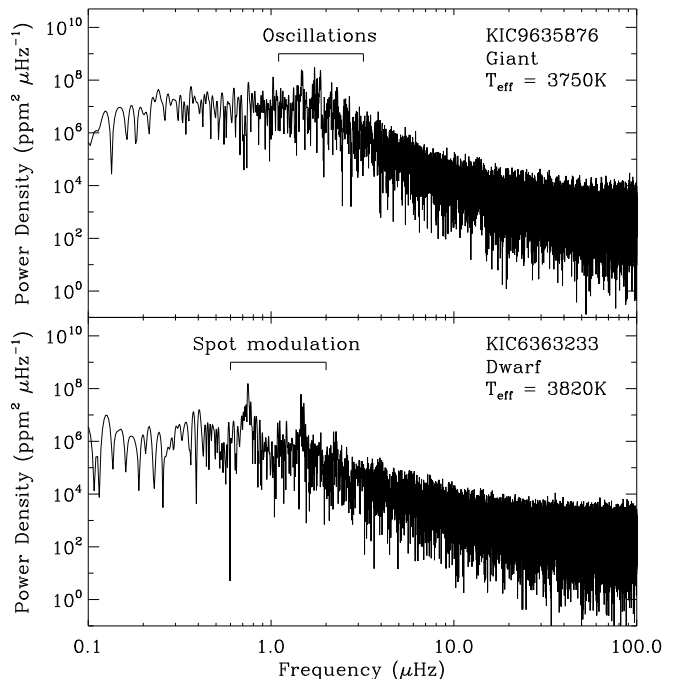


FIG. 7.— Comparison of long-cadence power spectra of a giant (top panel) and a dwarf (bottom panel) with similar effective temperatures in the sample by Mann et al. (2012). Note that KIC9635876 has been classified as a dwarf in the KIC.

this limit is about 3700 K, corresponding to a $\nu_{\text{max}} \sim 1 \mu\text{Hz}$ at solar metallicity. Second, there is evidence that tidal interactions from close stellar companions can suppress oscillations in giants, as first observed in the hierarchical triple system HD 180891 (Derekas et al. 2011; Borkovits et al. 2013; Fuller et al. 2013). Hence, giant stars that are also in multiple systems with close companions could escape a detection with our method.

To test the success rate of asteroseismic giant identifications, we analyzed 132 stars for which Mann et al. (2012) presented a spectroscopic luminosity class and for which several quarters of *Kepler* data are available. As an example, Figure 7 compares the power spectra of the dwarf KIC6363233 and the giant KIC9635876. The power spectrum of the dwarf shows a strong peak at $\sim 0.8 \mu\text{Hz}$ accompanied by several harmonics, a typical signature of non-sinusoidal variability due to rotational spot modulation. The giant, on the other hand, shows clear power excess with regularly spaced peaks that are typical for solar-like oscillations, indicating the evolved nature of the object. Out of the 132 stars in the sample, 96 were identified as giants based on detection of oscillations.

tions, compared to 104 stars that were identified as giants by Mann et al. (2012). All eight stars that were missed by the asteroseismic classification are cool ($\lesssim 3700$ K) giants, for which the oscillation timescales are likely too long to be resolved with the available amount of *Kepler* data. Hence, this result implies a very high success rate when T_{eff} restrictions are taken into account, and suggests that giants with suppressed oscillations by close-in stellar companions are rare.

As shown in Figure 4, our analysis did not yield a detection of oscillations compatible with giant stars in any of the cool main-sequence hosts. This confirms that the majority of these stars are indeed dwarfs. Additionally, we did not detect oscillations in stars near the 14 Gyr isochrone of the YY models (which can be seen as a “finger” between $T_{\text{eff}} = 4700 - 5000$ K and $\log g = 3.8 - 4.0$ in Figure 4). The non-detection of oscillations confirms that these stars must have $\log g \gtrsim 3.5$, and hence are either subgiants or cool dwarfs.

3.3. Stellar Density from Transit Measurements

The observation of transits allows a measurement of the semi-major axis as a function of the stellar radius (a/R_*), provided the eccentricity of the orbit is known. For the special case of circular orbits, a/R_* is directly related to the mean density of the star (see, e.g., Seager & Mallén-Ornelas 2003; Winn 2010):

$$\langle \rho_* \rangle \approx \frac{3\pi}{GP^2} \left(\frac{a}{R_*} \right)^3, \quad (5)$$

where G is the gravitational constant and P is the orbital period. Equation (5) can be used to infer host-star properties in systems with transiting exoplanets, for example to reduce degeneracies between spectroscopic parameters (see, e.g., Sozzetti et al. 2007; Torres et al. 2012).

Figure 8a compares the stellar densities derived from Equation (5) assuming $d/R_* = a/R_*$ in the table of Batalha et al. (2013) with our independent estimates from asteroseismology. We emphasize that Batalha et al. (2013) explicitly report the quantity d/R_* to point out that it is only a valid measurement of stellar density in the case of zero eccentricity, for which $d/R_* = a/R_*$. We also note that the uncertainties reported by Batalha et al. (2013) do not account for correlations between transit parameters, and hence the density uncertainties are likely underestimated. For this first comparison, we have excluded all hosts with a transit density uncertainty $> 50\%$.

The comparison shows differences greater than 50% for more than half of the sample, with mostly underestimated stellar densities from the transit model compared to the seismic densities. To investigate the cause of this discrepancy, Figure 8b shows the fractional difference of stellar densities as a function of the impact parameter (the sky-projected distance of the planet to center of the stellar disc, expressed in units of the stellar radius) for each planet candidate. We observe a clear correlation, with large disagreements corresponding preferentially to high impact parameters. We have tested whether this bias is due to insufficiently sampled ingress and egress times by repeating the transit fits for a fraction of the host stars using short-cadence data, and found that the agreement significantly improves if short-cadence data is

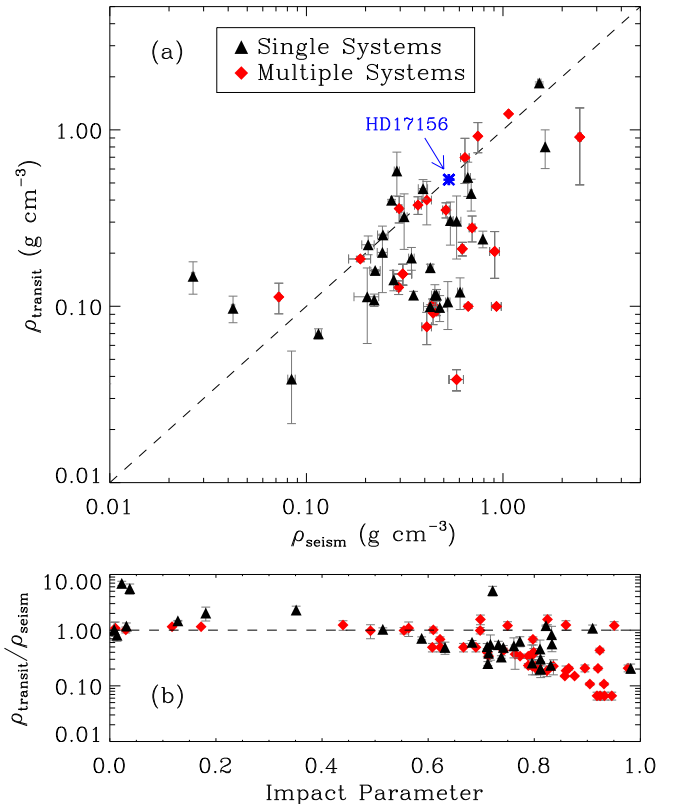


FIG. 8.— (a) Mean stellar density as measured from the transit assuming circular orbits ($d/R_* = a/R_*$) versus the density measured from asteroseismology. (b) Fractional difference between the density measured from the transit and asteroseismology as a function of the modeled impact parameter. Note that since all planets are assumed to orbit the same star, panel (a) shows one datapoint for each host star, while panel (b) shows one datapoint for each planet candidate.

used. Further investigation showed that the larger disagreements are found for the shallower transits, while better agreement is found for transits with the highest S/N. Hence, it appears that impact parameters tend to be overestimated for small planets, which is compensated by underestimating the density of the star to match the observed transit duration. The reason for this bias may be due to anomalously long ingress times for small planets caused by smearing due to uncorrected transit timing variations or other effects.

Additional reasons for the discrepancies between the transit and seismic densities include planet candidates on eccentric orbits, and false-positive planet candidates. For eccentric orbits the stellar density derived from the transit can be either over- or underestimated (depending on the orientation of the orbit to the observer). However, in this case no correlation with the impact parameter would be expected, and the distribution of impact parameters should be uniform. Additionally, if eccentric orbits were responsible for the majority of the outliers, we would expect to detect a correlation of the fractional difference in density with orbital period, with planet candidates on short orbital periods showing preferentially good agreement due to tidal circularization. However, no such correlation is apparent in our data. For false-positive scenarios (e.g. a transit around a fainter background star) the large dilution would lead to underesti-

mated densities, and a correlation with the impact parameter would be expected. However, recent results by Fressin et al. (2013) showed that the global false-positive rate is $\lesssim 10\%$. Hence, eccentric orbits and false-positives are likely not responsible for the majority of the outliers.

The first comparison shown here underlines the statement in Batalha et al. (2013) that stellar properties derived from the transit fits in the planet-candidate catalog should be viewed with caution, with further work being needed to quantify these differences. We emphasize that the comparison shown here does not imply that transits cannot be used to accurately infer stellar densities. To demonstrate this, Figure 8a also includes HD 17156, a system with an exoplanet in a highly eccentric orbit ($e = 0.68$) for which high S/N constraints from transits, radial velocities and asteroseismology are available (Gilliland et al. 2011; Nutzman et al. 2011). The seismic and transit density are in excellent agreement, demonstrating that both techniques yield consistent results when the eccentricity and impact parameter can be accurately determined. Similar tests can be expected in future studies, making use of *Kepler* exoplanet hosts for which asteroseismic and radial velocity constraints are available (Batalha et al. 2011; Gilliland et al. 2013; Marcy et al. 2013). Additionally, the precise stellar properties presented here will enable improved determinations of eccentricities using high S/N transit light curves (Dawson & Johnson 2012), and yield improved constraints for the study of eccentricity distributions in the *Kepler* planet sample compared to planets detected with radial velocities (see, e.g., Wang & Ford 2011; Moorhead et al. 2011; Kane et al. 2012; Plavchan et al. 2012)

4. EXOPLANET – HOST STAR CORRELATIONS

Accurate stellar properties of exoplanet hosts, as presented in this study, are valuable for testing theories of planet formation, many of which are related to host-star properties. While both the limited sample size and the difficult characterization of detection biases push a comprehensive investigation of exoplanet – host star correlations beyond the scope of this paper, we present a first qualitative comparison here. Note that in the following we have omitted planet candidates that have been identified as false positives (see Section 3.1) or for which unpublished radial-velocity follow-up has indicated a low-mass stellar companion (see Table 3).

4.1. Background

The favored theoretical scenario for the formation of terrestrial planets and the cores of gas giants is the core-accretion model, a slow process involving the collision of planetesimals (Safronov & Zvjagina 1969), with giant planets growing massive enough to gravitationally trap light gases (Mizuno 1980; Pollack et al. 1996; Lissauer et al. 2009; Movshovitz et al. 2010). The efficiency of this process is predicted to be correlated with the disk properties and therefore the characteristics of the host star, such as stellar mass (Thommes et al. 2008).

Observationally, Doppler velocity surveys have yielded two important correlations: gas giant planets occur more frequently around stars of high metallicity (Gonzalez 1997; Santos et al. 2004; Fischer & Valenti 2005) and around more massive stars (Laws et al. 2003;

Johnson et al. 2007; Lovis & Mayor 2007; Johnson et al. 2010). Early results using *Kepler* planet candidates showed that single planets appear to be more common around hotter stars, while multiple planetary system are preferentially found around cooler stars (Latham et al. 2011). Both results are in-line with Howard et al. (2012), who found that small planets are more common around cool stars. More recently, Steffen et al. (2012a) showed evidence that hot Jupiters indeed tend to be found in single planet systems, while Fressin et al. (2013) found that the occurrence of small planets appears to be independent of the host-star spectral type. While most of these findings have been interpreted in favor of the core-accretion scenario, many results have so far relied on uncertain or indirect estimates of stellar mass (such as T_{eff}). The sample of host stars presented in this study allow us to test these results using accurate radii and masses from asteroseismology.

4.2. Planet Radius versus Stellar Mass

Following Howard et al. (2012), we attempted to account for detection biases by estimating the smallest detectable planet for a given planet-candidate host in our sample as:

$$R_{\text{min}} = R_{\star} (\text{SNR } \sigma_{\text{CDPP}})^{0.5} \left(\frac{n_{\text{tr}} t_{\text{dur}}}{6\text{hr}} \right)^{0.25}. \quad (6)$$

Here, R_{\star} is the host-star radius, SNR is the required signal-to-noise ratio, σ_{CDPP} is the 6 hr combined differential photometric precision (Christiansen et al. 2012), n_{tr} is the number of transits observed and t_{dur} is the duration of the transits which, for the simplified case of circular orbits and a central transit (impact parameter $b = 0$), is given by:

$$t_{\text{dur}} = \frac{R_{\star} P}{\pi a}. \quad (7)$$

Here, P is the orbital period and a is the semi-major axis of the orbit. For each candidate, we estimate R_{min} by calculating t_{dur} , adopting the median 6 hr σ_{CDPP} from quarters 1–6 for each star and setting a signal-to-noise threshold of 25 (Ciardi et al. 2013). To de-bias our sample, we calculated for a range of planet sizes R_x the number of planet candidates that are larger than R_x and for which $R_{\text{min}} < R_x$. The maximum number of planet candidates fulfilling these criteria was found for a value of $R_x = 2.4R_{\oplus}$. In the following, our debiased sample consists only of planet candidates with $R > 2.4R_{\oplus}$ and with $R_{\text{min}} < 2.4R_{\oplus}$. Figure 9a shows planet radii versus host-star mass for all planet candidates in our sample (grey symbols), with the de-biased sample shown as filled symbols. Planet candidates in multi systems are shown as diamonds, while single systems are shown as triangles. For all candidates in the debiased sample, symbols are additionally color-coded according to the incident flux as a multiple of the flux incident on Earth.

While the size of our de-biased sample precludes definite conclusions, we see that our observations are consistent with previous studies that found gas-giant planets to be less common around low-mass stars ($< 1M_{\odot}$) than around more massive stars. A notable exception is KOI-1 (TReS-2), a $0.9 M_{\odot}$ K-dwarf hosting a hot Jupiter

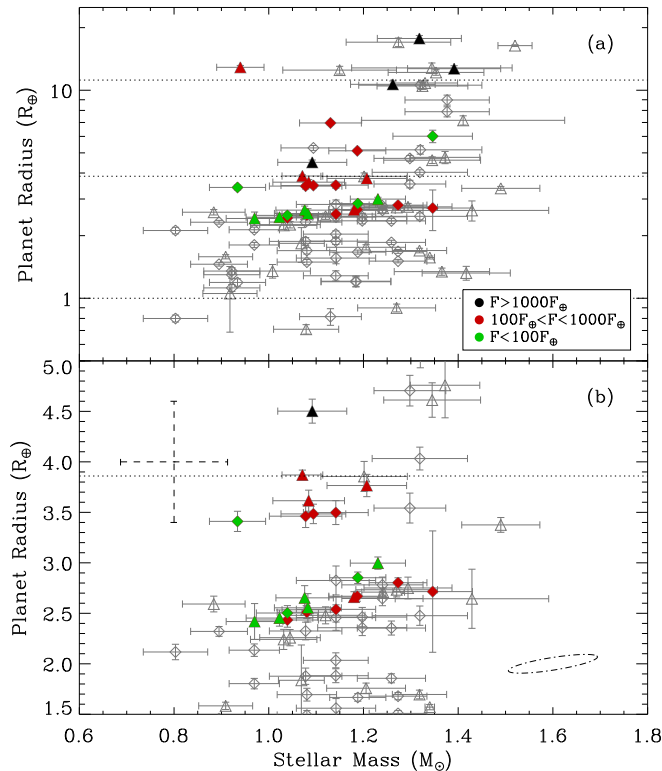


FIG. 9.— (a) Planet radius versus host-star mass for all planet-candidate hosts in our sample. Planet candidates with radii $> 2.4 R_{\oplus}$ and $R_{\min} < 2.4 R_{\oplus}$ are shown as filled symbols, while other candidates are shown as open grey symbols. Triangles and diamonds denote candidates in single and multiple systems, respectively. Colors denote the incident stellar flux, as indicated in the legend. Horizontal dotted lines show the sizes of Earth, Neptune and Jupiter. (b) Same as panel (a) but only showing candidates with radii between 1.5 and $5 R_{\oplus}$. The dashed error bar shows typical $1 - \sigma$ uncertainties without asteroseismic constraints. The dashed-dotted line shows a typical $1 - \sigma$ error ellipse, illustrating the correlation of uncertainties between stellar mass and planet radius in the asteroseismic sample.

in a 2.5-day orbit (O’Donovan et al. 2006; Holman et al. 2007; Kipping & Bakos 2011; Barclay et al. 2012). However, this observation is only marginally significant: considering the full sample of stars hosting planet candidates with $R > 4 R_{\oplus}$, the probability of observing one host with $M < 1 M_{\odot}$ by chance is $\sim 1\%$, corresponding to a $\sim 2.5\sigma$ significance that the mass distribution is different. Using our unbiased sample, no statistically significant difference is found.

For sub-Neptune sized objects, planet candidates are detected around stars with masses ranging over the full span of our sample ($\sim 0.8 - 1.6 M_{\odot}$). This is illustrated in Figure 9b, showing a close-up of the region of sub-Neptune planets on a linear scale. To demonstrate the improvement of the uncertainties in our sample, the dashed lines in Figure 9b shows an error bar for a typical best-case scenario when host-star properties are based on spectroscopy alone (10% in stellar mass and 15% in stellar radius, Basu et al. 2012), neglecting uncertainties arising from the measurement of the transit depth. We note that, strictly speaking, the uncertainties in stellar mass and planet radius are not independent since asteroseismology constrains mostly the mean stellar density. The dashed-dotted line in Figure 9b illustrates this

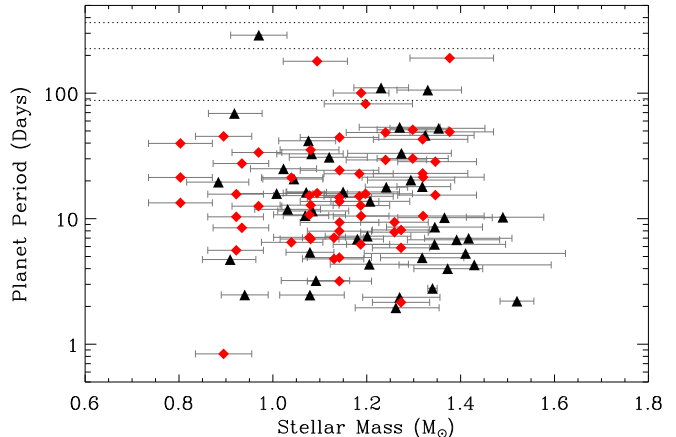


FIG. 10.— Orbital period versus stellar mass for all planet candidates in our sample. Black triangles are candidates in single systems and red diamonds are candidates in multiple systems. The orbital periods of Mercury, Venus and Earth are shown as horizontal dotted lines.

by showing an error ellipse calculated from Monte-Carlo simulations for a typical host-planet pair in our sample.

The data in Figure 9b show a tentative lack of planets with sizes close to $3 R_{\oplus}$, which does not seem to be related to detection bias in the sample. While this gap is intriguing, it is not compatible with previous observations of planets with radii between $3 - 3.5 R_{\oplus}$, such as in the Kepler-11 system (Lissauer et al. 2011). Further observations will be needed to determine whether the apparent gap in Figure 9b is real or simply a consequence of the small size of the available sample.

4.3. Planet Period and Multiplicity versus Stellar Mass

The second main observable that can be tested for correlations with the host-star mass is the orbital period of the planet candidates. Here, we do not expect a detection bias to be correlated with the host-star properties, and hence we consider the full sample. Figure 10 compares the orbital period of the planet candidates as a function of host-star mass. There does not appear to be an overall trend, although there is a tendency for more single-planet candidates (black triangles) in close orbits (< 10 days) around higher mass ($\gtrsim 1.3 M_{\odot}$) stars. This observation would qualitatively be consistent with previous findings that hot-Jupiters are rare in multiple planet systems and are more frequently found around higher mass stars. However, we note that roughly half of the planet candidates with periods less than 10 days around stars with $M > 1.3 M_{\odot}$ have radii smaller than Neptune, and two have radii smaller than $2 R_{\oplus}$ (see also Figure 9). Additionally, a K-S test yields only a marginal statistical difference ($\sim 2.4\sigma$) between host-star masses of single and multiple planet systems for periods < 10 days.

5. CONCLUSIONS

We have presented an asteroseismic study of *Kepler* planet-candidate host stars in the catalog by Batalha et al. (2013). Our analysis yields new asteroseismic radii and masses for 66 host stars with typical uncertainties of 3% and 7%, respectively, raising the total number of *Kepler* host stars with asteroseismic solutions to 77. Our main findings can be summarized as follows:

1. Surface gravities for subgiant and giant host stars in Batalha et al. (2013) based on high-resolution spectroscopy are systematically overestimated, yielding underestimated stellar radii (and hence planet-candidate radii) by up to a factor of 1.5. While properties for unevolved stars based on spectroscopy are in good agreement and show greatly improved results compared to the KIC, the identified systematics illustrate the importance of combining spectroscopy with asteroseismic constraints to derive accurate and precise host-star properties.
2. We have demonstrated that asteroseismology is an efficient method to identify giants using *Kepler* data. Our analysis yielded no detection of oscillations in host stars classified as M dwarfs, confirming that the fraction of misclassified giants in the cool planet-candidate host-star sample is small. An extension of this analysis to the complete *Kepler* target sample is planned, and will support completeness studies of *Kepler* planet detections and hence the determination of the frequency of Earth-sized planets in the habitable zone.
3. A comparison of mean stellar densities from asteroseismology and from transit models in Batalha et al. (2013), assuming zero eccentricity, showed significant differences for at least 50% of the sample. Preliminary investigations imply that these differences are mostly due to systematics in the modeled transit parameters, while some differences may be due to planet candidates in eccentric orbits. The independent asteroseismic densities presented here will be valuable for more detailed studies of the intrinsic eccentricity distribution of planets in this sample and for testing densities inferred from transits for planet-candidate host stars with available radial-velocity data.
4. We presented re-derived radii and semi-major axes for the 107 planet candidates in our sample based on the revised host-star properties. We identified KOI-1230.01 and KOI-2481.01 as astrophysical false-positives, with revised companion radii of $64 \pm 2 R_{\oplus}$ ($0.58 \pm 0.02 R_{\odot}$), $31 \pm 2 R_{\oplus}$ ($0.29 \pm 0.02 R_{\odot}$), respectively, while KOI-2640.01 is a potential false-positive with a radius of $17.0 \pm 0.8 R_{\oplus}$. On the other hand, the radius of KOI-1894.01 decreases from the brown-dwarf/stellar regime to a sub-Jupiter size ($7.2 \pm 0.4 R_{\oplus}$). Our sample also includes accurate asteroseismic radii and masses for four hosts with confirmed planets: Kepler-4, Kepler-14, Kepler-23 and Kepler-25.
5. We investigated correlations between host-star

masses and planet-candidate properties, and find that our observations are consistent with previous studies showing that gas giants are less common around lower-mass ($\lesssim 1M_{\odot}$) stars. Sub-Neptune sized planets, on the other hand, appear to be found over the full range of host masses considered in this study ($\sim 0.8 - 1.6 M_{\odot}$). We also observe a potential preference for close-in planets around higher mass stars to be in single systems. Due to the small sample size, however, these findings are tentative only and will have to await confirmation using larger samples with precise host-star properties.

The results presented here illustrate the powerful synergy between asteroseismology and exoplanet studies. As the *Kepler* mission progresses, asteroseismology will continue to play an important role in characterizing new *Kepler* planet candidates, particularly for potential long-period planets in the habitable zones of F-K dwarfs. An important future step will also be to extend the sample of planets with determined masses through radial velocity follow-up (see, e.g., Latham et al. 2010; Cochran et al. 2011) or transit-timing variations (see, e.g., Fabrycky et al. 2012; Ford et al. 2012; Steffen et al. 2012b) for hosts for which asteroseismic constraints are available. This will enable precise constraints on planet densities. Additionally, the analysis of individual frequencies for planet-candidate hosts with high S/N detections will allow the precise determination of stellar ages, which can be used to investigate the chronology of their planetary systems.

ACKNOWLEDGMENTS

We thank Willie Torres, Josh Winn and our anonymous referee for helpful comments and discussions. We furthermore gratefully acknowledge the entire *Kepler* team and everyone involved in the *Kepler* mission for making this paper possible. Funding for the *Kepler* Mission is provided by NASA's Science Mission Directorate. DH is supported by an appointment to the NASA Postdoctoral Program at Ames Research Center, administered by Oak Ridge Associated Universities through a contract with NASA. SB acknowledges NSF grant AST-1105930. SH acknowledges financial support from the Netherlands Organisation for Scientific Research (NWO). TSM acknowledges NASA grant NNX13AE91G. Funding for the Stellar Astrophysics Centre is provided by The Danish National Research Foundation (Grant DNR106). The research is supported by the ASTERISK project (ASTERoseismic Investigations with SONG and Kepler) funded by the European Research Council (Grant agreement no.: 267864).

REFERENCES

- Aerts, C., Christensen-Dalsgaard, J., & Kurtz, D. W. 2010, *Asteroseismology* (Springer: Dordrecht)
- Barclay, T., et al. 2012, *ApJ*, 761, 53
- . 2013, *Nature*, 494, 452
- Basu, S., Chaplin, W. J., & Elsworth, Y. 2010, *ApJ*, 710, 1596
- Basu, S., Verner, G. A., Chaplin, W. J., & Elsworth, Y. 2012, *ApJ*, 746, 76
- Basu, S., et al. 2011, *ApJ*, 729, L10
- Batalha, N. M., et al. 2011, *ApJ*, 729, 27
- . 2013, *ApJS*, 204, 24
- Bedding, T. R. 2011, *ArXiv e-prints* (arXiv:1107.1723)
- Bedding, T. R., et al. 2010, *ApJ*, 713, L176
- Belkacem, K. 2012, in SF2A-2012: Proceedings of the Annual meeting of the French Society of Astronomy and Astrophysics, ed. S. Boissier, P. de Laverny, N. Nardetto, R. Samadi, D. Valls-Gabaud, & H. Wozniak, 173–188

- Belkacem, K., Goupil, M. J., Dupret, M. A., Samadi, R., Baudin, F., Noels, A., & Mosser, B. 2011, *A&A*, 530, A142
- Borkovits, T., et al. 2013, *MNRAS*, 428, 1656
- Borucki, W. J., et al. 2010a, *ApJ*, 713, L126
- 2010b, *Science*, 327, 977
- 2011a, *ApJ*, 728, 117
- 2011b, *ApJ*, 736, 19
- 2012, *ApJ*, 745, 120
- Bouchy, F., Bazot, M., Santos, N. C., Vauclair, S., & Sosnowska, D. 2005, *A&A*, 440, 609
- Brogaard, K., et al. 2012, *A&A*, 543, A106
- Brown, T. M., & Gilliland, R. L. 1994, *ARA&A*, 32, 37
- Brown, T. M., Gilliland, R. L., Noyes, R. W., & Ramsey, L. W. 1991, *ApJ*, 368, 599
- Brown, T. M., Latham, D. W., Everett, M. E., & Esquerdo, G. A. 2011, *AJ*, 142, 112
- Bruntt, H., et al. 2012, *MNRAS*, 423, 122
- Buchhave, L. A., et al. 2011, *ApJS*, 197, 3
- 2012, *Nature*, 486, 375
- Carter, J. A., et al. 2012, *Science*, 337, 556
- Casagrande, L., Ramírez, I., Meléndez, J., Bessell, M., & Asplund, M. 2010, *A&A*, 512, A54
- Chaplin, W. J., et al. 2011a, *Science*, 332, 213
- 2011b, *ApJ*, 732, 54
- 2013, *ApJ*, 766, 101
- Christensen-Dalsgaard, J. 2004, *Sol. Phys.*, 220, 137
- Christensen-Dalsgaard, J. 2008, *Ap&SS*, 316, 13
- Christensen-Dalsgaard, J., et al. 2010, *ApJ*, 713, L164
- Christiansen, J. L., et al. 2012, *PASP*, 124, 1279
- Ciardi, D. R., Fabrycky, D. C., Ford, E. B., Gautier, III, T. N., Howell, S. B., Lissauer, J. J., Ragozzine, D., & Rowe, J. F. 2013, *ApJ*, 763, 41
- Cochran, W. D., et al. 2011, *ApJS*, 197, 7
- Creevey, O. L., et al. 2012, *A&A*, 537, A111
- da Silva, L., et al. 2006, *A&A*, 458, 609
- Dawson, R. I., & Johnson, J. A. 2012, *ApJ*, 756, 122
- Demarque, P., Guenther, D. B., Li, L. H., Mazumdar, A., & Straka, C. W. 2008, *Ap&SS*, 316, 31
- Demarque, P., Woo, J.-H., Kim, Y.-C., & Yi, S. K. 2004, *ApJS*, 155, 667
- Derekas, A., et al. 2011, *Science*, 332, 216
- di Mauro, M. P., et al. 2011, *MNRAS*, 415, 3783
- Djupvik, A. A., & Andersen, J. 2010, in *Highlights of Spanish Astrophysics V*, ed. J. M. Diego, L. J. Goicoechea, J. I. González-Serrano, & J. Gorgas, 211
- Dotter, A., Chaboyer, B., Jevremović, D., Kostov, V., Baron, E., & Ferguson, J. W. 2008, *ApJS*, 178, 89
- Doğan, G., Brandão, I. M., Bedding, T. R., Christensen-Dalsgaard, J., Cunha, M. S., & Kjeldsen, H. 2010, *Ap&SS*, 328, 101
- Fabrycky, D. C., et al. 2012, *ApJ*, 750, 114
- Fischer, D. A., & Valenti, J. 2005, *ApJ*, 622, 1102
- Ford, E. B., et al. 2012, *ApJ*, 750, 113
- Fressin, F., et al. 2013, *ApJ*, 766, 81
- Fuller, J., Derekas, A., Borkovits, T., Huber, D., Bedding, T. R., & Kiss, L. L. 2013, *MNRAS*, 429, 2425
- Fűrész, G. 2008, PhD thesis, University of Szeged, Szeged, Hungary
- Gai, N., Basu, S., Chaplin, W. J., & Elsworth, Y. 2011, *ApJ*, 730, 63
- Gaidos, E., & Mann, A. W. 2013, *ApJ*, 762, 41
- Gautier, III, T. N., et al. 2010, *ArXiv e-prints* (arXiv:1001.0352)
- Gilliland, R. L., McCullough, P. R., Nelan, E. P., Brown, T. M., Charbonneau, D., Nutzman, P., Christensen-Dalsgaard, J., & Kjeldsen, H. 2011, *ApJ*, 726, 2
- Gilliland, R. L., et al. 2010a, *ApJ*, 713, L160
- 2010b, *PASP*, 122, 131
- 2013, *ApJ*, 766, 40
- Gonzalez, G. 1997, *MNRAS*, 285, 403
- Gough, D. O. 1986, in *Hydrodynamic and Magnetodynamic Problems in the Sun and Stars*, ed. Y. Osaki (Uni. of Tokyo Press), 117
- Hekker, S., et al. 2009, *A&A*, 506, 465
- 2010, *MNRAS*, 402, 2049
- 2011a, *MNRAS*, 414, 2594
- 2011b, *A&A*, 525, A131
- 2012, *A&A*, 544, A90
- Holman, M. J., et al. 2007, *ApJ*, 664, 1185
- Houdek, G. 2006, in *ESA Special Publication, Vol. 624, Proceedings of SOHO 18/GONG 2006/HELAS I, Beyond the spherical Sun*
- Huber, G., Balmforth, N. J., Christensen-Dalsgaard, J., & Gough, D. O. 1999, *A&A*, 351, 582
- Howard, A. W., et al. 2012, *ApJS*, 201, 15
- Howell, S. B., et al. 2012, *ApJ*, 746, 123
- Huber, D., Stello, D., Bedding, T. R., Chaplin, W. J., Arentoft, T., Quirion, P.-O., & Kjeldsen, H. 2009, *Communications in Asteroseismology*, 160, 74
- Huber, D., et al. 2010, *ApJ*, 723, 1607
- 2011, *ApJ*, 743, 143
- 2012, *ApJ*, 760, 32
- 2013, in preparation
- Jenkins, J. M., et al. 2010, *ApJ*, 713, L120
- Jiang, C., et al. 2011, *ApJ*, 742, 120
- Johnson, J. A., Aller, K. M., Howard, A. W., & Crepp, J. R. 2010, *PASP*, 122, 905
- Johnson, J. A., Butler, R. P., Marcy, G. W., Fischer, D. A., Vogt, S. S., Wright, J. T., & Peek, K. M. G. 2007, *ApJ*, 670, 833
- Johnson, J. A., et al. 2012, *AJ*, 143, 111
- Kallinger, T., et al. 2010a, *A&A*, 522, A1
- 2010b, *A&A*, 509, A77
- Kane, S. R., Ciardi, D. R., Gelino, D. M., & von Braun, K. 2012, *MNRAS*, 425, 757
- Karoff, C., Campante, T. L., & Chaplin, W. J. 2010, *ArXiv e-prints* (arXiv:1003.4167)
- Kipping, D., & Bakos, G. 2011, *ApJ*, 733, 36
- Kjeldsen, H., & Bedding, T. R. 1995, *A&A*, 293, 87
- Koch, D. G., et al. 2010, *ApJ*, 713, L79
- Latham, D. W., et al. 2010, *ApJ*, 713, L140
- 2011, *ApJ*, 732, L24
- Laws, C., Gonzalez, G., Walker, K. M., Tyagi, S., Dodsworth, J., Snider, K., & Suntzeff, N. B. 2003, *AJ*, 125, 2664
- Lissauer, J. J., Hubickyj, O., D'Angelo, G., & Bodenheimer, P. 2009, *Icarus*, 199, 338
- Lissauer, J. J., et al. 2011, *Nature*, 470, 53
- Lovis, C., & Mayor, M. 2007, *A&A*, 472, 657
- Lund, M. N., Chaplin, W. J., & Kjeldsen, H. 2012, *MNRAS*, 427, 1784
- Mann, A. W., Gaidos, E., Lépine, S., & Hilton, E. J. 2012, *ApJ*, 753, 90
- Marcy, G. W., et al. 2013, in preparation
- Marigo, P., Girardi, L., Bressan, A., Groenewegen, M. A. T., Silva, L., & Granato, G. L. 2008, *A&A*, 482, 883
- Mathur, S., et al. 2012, *ApJ*, 749, 152
- Metcalfe, T. S., et al. 2010, *ApJ*, 723, 1583
- 2012, *ApJ*, 748, L10
- Miglio, A. 2012, in *Red Giants as Probes of the Structure and Evolution of the Milky Way*, ed. A. Miglio, J. Montalbán, & A. Noels, *ApSS Proceedings*
- Miglio, A., Morel, T., Barbieri, M., Mosser, B., Girardi, L., Montalbán, J., & Valentini, M. 2012a, in *European Physical Journal Web of Conferences, Vol. 19, European Physical Journal Web of Conferences*, 5012
- Miglio, A., et al. 2009, *A&A*, 503, L21
- 2012b, *MNRAS*, 419, 2077
- 2013a, *ArXiv e-prints* (arXiv:1301.1515)
- 2013b, *MNRAS*, 429, 423
- Mizuno, H. 1980, *Progress of Theoretical Physics*, 64, 544
- Molenda-Zakowicz, J., Latham, D. W., Catanzaro, G., Frasca, A., & Quinn, S. N. 2011, *MNRAS*, 412, 1210
- Moorhead, A. V., et al. 2011, *ApJS*, 197, 1
- Morel, T., & Miglio, A. 2012, *MNRAS*, 419, L34
- Mosser, B., et al. 2010, *A&A*, 517, A22
- 2012, *A&A*, 537, A30
- 2013, *A&A*, 550, A126
- Movshovitz, N., Bodenheimer, P., Podolak, M., & Lissauer, J. J. 2010, *Icarus*, 209, 616
- Muirhead, P. S., Hamren, K., Schlawin, E., Rojas-Ayala, B., Covey, K. R., & Lloyd, J. P. 2012a, *ApJ*, 750, L37
- Muirhead, P. S., et al. 2012b, *ApJ*, 747, 144
- Nutzman, P., et al. 2011, *ApJ*, 726, 3
- O'Donovan, F. T., et al. 2006, *ApJ*, 651, L61

- Pietrinferni, A., Cassisi, S., Salaris, M., & Castelli, F. 2004, *ApJ*, 612, 168
- Pinsonneault, M. H., An, D., Molenda-Żakowicz, J., Chaplin, W. J., Metcalfe, T. S., & Bruntt, H. 2012, *ApJS*, 199, 30
- Plavchan, P., Bilinski, C., & Currie, T. 2012, *ArXiv e-prints* (arXiv:1203.1887)
- Pollack, J. B., Hubickyj, O., Bodenheimer, P., Lissauer, J. J., Podolak, M., & Greenzweig, Y. 1996, *Icarus*, 124, 62
- Safronov, V. S., & Zvjagina, E. V. 1969, *Icarus*, 10, 109
- Samadi, R., Georgobiani, D., Trampedach R., R., Goupil, M. J., Stein, R. F., & Nordlund, A. 2007, *A&A*, 463, 297
- Santos, N. C., Israelian, G., & Mayor, M. 2004, *A&A*, 415, 1153
- Savitzky, A., & Golay, M. J. E. 1964, *Analytical Chemistry*, 36, 1627
- Seager, S., & Mallén-Ornelas, G. 2003, *ApJ*, 585, 1038
- Silva Aguirre, V., et al. 2011, *ApJ*, 740, L2
- . 2012, *ApJ*, 757, 99
- . 2013, *ApJ*, submitted
- Southworth, J. 2011, *MNRAS*, 417, 2166
- . 2012, *MNRAS*, 426, 1291
- Sozzetti, A., Torres, G., Charbonneau, D., Latham, D. W., Holman, M. J., Winn, J. N., Laird, J. B., & O'Donovan, F. T. 2007, *ApJ*, 664, 1190
- Steffen, J. H., et al. 2012a, *Proceedings of the National Academy of Science*, 109, 7982
- . 2012b, *MNRAS*, 421, 2342
- Stello, D., Bruntt, H., Preston, H., & Buzasi, D. 2008, *ApJ*, 674, L53
- Stello, D., et al. 2009, *ApJ*, 700, 1589
- Tassoul, M. 1980, *ApJS*, 43, 469
- Thommes, E. W., Matsumura, S., & Rasio, F. A. 2008, *Science*, 321, 814
- Thygesen, A. O., et al. 2012, *A&A*, 543, A160
- Torres, G., Fischer, D. A., Sozzetti, A., Buchhave, L. A., Winn, J. N., Holman, M. J., & Carter, J. A. 2012, *ApJ*, 757, 161
- Ulrich, R. K. 1986, *ApJ*, 306, L37
- Valenti, J. A., & Piskunov, N. 1996, *A&AS*, 118, 595
- Vandakurov, Y. V. 1968, *Soviet Ast.*, 11, 630
- Vauclair, S., Laymand, M., Bouchy, F., Vauclair, G., Hui Bon Hoa, A., Charpinet, S., & Bazot, M. 2008, *A&A*, 482, L5
- Verner, G. A., & Roxburgh, I. W. 2011, *ArXiv e-prints* (arXiv:1104.0631)
- Verner, G. A., et al. 2011a, *MNRAS*, 415, 3539
- . 2011b, *ApJ*, 738, L28
- Vogt, S. S., et al. 1994, in *Society of Photo-Optical Instrumentation Engineers (SPIE) Conference Series*, Vol. 2198, *Society of Photo-Optical Instrumentation Engineers (SPIE) Conference Series*, ed. D. L. Crawford & E. R. Craine, 362
- Wang, J., & Ford, E. B. 2011, *MNRAS*, 418, 1822
- White, T. R., Bedding, T. R., Stello, D., Christensen-Dalsgaard, J., Huber, D., & Kjeldsen, H. 2011, *ApJ*, 743, 161
- Winn, J. N. 2010, *ArXiv e-prints* (arXiv:1001.2010)
- Wright, D. J., et al. 2011, *ApJ*, 728, L20

TABLE 1 Asteroseismic and Spectroscopic Observations of 77 *Kepler* Planet-Candidate Hosts.

KOI	KIC	Kp	Asteroseismology					Spectroscopy					Notes
			ν_{\max} (μHz)	$\Delta\nu$ (μHz)	HBR	M	Cad	$v \sin(i)$	S/N	CCF	Sp	Obs	
1	11446443	11.34	–	141.0 \pm 1.4	–	25	SC	–	–	–	–	–	Kepler-1 ^a
2	10666592	10.46	–	59.22 \pm 0.59	–	1	SC	–	–	–	–	–	Kepler-2 ^b
5	8554498	11.66	1153 \pm 76	61.98 \pm 0.96	1.079	30	SC	10.3 \pm 0.5	167	0.978	3	HM	–
7	11853905	12.21	1436 \pm 42	74.4 \pm 1.1	1.080	25	SC	2.3 \pm 0.5	168	0.971	5	FH	Kepler-4
41	6521045	11.20	1502 \pm 31	77.0 \pm 1.1	1.215	27	SC	2.9 \pm 0.5	300	0.987	5	HM	–
42	8866102	9.36	2014 \pm 32	94.50 \pm 0.60	1.348	28	SC	15.0 \pm 0.5	176	0.968	2	HM	–
64	7051180	13.14	681 \pm 19	40.05 \pm 0.54	1.100	27	SC	2.4 \pm 0.5	131	0.985	3	H	–
69	3544595	9.93	3366 \pm 81	145.77 \pm 0.45	1.036	28	SC	2.0 \pm 0.5	175	0.986	10	FHM	–
72	11904151	10.96	–	118.20 \pm 0.20	–	5	SC	–	–	–	–	–	Kepler-10 ^c
75	7199397	10.78	643 \pm 17	38.63 \pm 0.68	1.859	28	SC	5.6 \pm 0.5	91	0.964	5	HMT	–
85	5866724	11.02	1880 \pm 60	89.56 \pm 0.48	–	27	SC	–	–	–	–	–	Kepler-50 ^d
87	10593626	11.66	–	137.5 \pm 1.4	–	18	SC	–	–	–	–	–	Kepler-22 ^e
97	5780885	12.88	–	56.4 \pm 1.7	1.050	18	SC	3.3 \pm 0.5	73	0.975	10	FM	–
98	10264660	12.13	–	53.9 \pm 1.6	1.078	27	SC	10.8 \pm 0.5	89	0.970	10	FH	Kepler-14
107	11250587	12.70	–	74.4 \pm 2.8	1.035	18	SC	3.3 \pm 0.7	39	0.889	2	F	–
108	4914423	12.29	1663 \pm 56	81.5 \pm 1.6	1.062	27	SC	3.8 \pm 0.7	108	0.945	5	HM	–
113	2306756	12.39	1412 \pm 50	70.4 \pm 2.2	1.054	12	SC	2.5 \pm 0.5	25	0.915	3	FMT	–
117	10875245	12.49	1711 \pm 107	86.7 \pm 3.7	1.043	21	SC	3.5 \pm 0.5	39	0.978	2	M	–
118	3531558	12.38	–	86.8 \pm 2.2	1.042	18	SC	2.2 \pm 0.5	25	0.894	1	F	–
119	9471974	12.65	–	49.4 \pm 3.2	1.052	12	SC	5.3 \pm 0.6	27	0.871	3	F	–
122	8349582	12.35	1677 \pm 90	83.6 \pm 1.4	1.061	27	SC	2.3 \pm 0.5	107	0.973	5	HM	–
123	5094751	12.37	1745 \pm 117	91.1 \pm 2.3	1.046	27	SC	2.8 \pm 0.5	117	0.963	6	HM	–
168	11512246	13.44	–	72.9 \pm 2.1	1.026	27	SC	2.9 \pm 0.5	24	0.850	2	FM	Kepler-23
244	4349452	10.73	2106 \pm 50	98.27 \pm 0.57	1.082	22	SC	11.1 \pm 0.5	123	0.939	5	HMT	Kepler-25
245	8478994	9.71	–	178.7 \pm 1.4	–	15	SC	–	–	–	–	–	Kepler-37 ^f
246	11295426	10.00	2154 \pm 13	101.57 \pm 0.10	–	22	SC	–	–	–	–	–	Kepler-68 ^g
257	5514383	10.87	–	113.3 \pm 2.0	1.081	16	SC	9.4 \pm 0.5	41	0.909	4	MT	–
260	8292840	10.50	1983 \pm 37	92.85 \pm 0.35	1.219	21	SC	10.4 \pm 0.5	47	0.868	3	MT	–
262	11807274	10.42	1496 \pm 56	75.71 \pm 0.31	–	18	SC	–	–	–	–	–	Kepler-65 ^d
263	10514430	10.82	1303 \pm 30	70.0 \pm 1.0	1.077	22	SC	2.7 \pm 0.6	101	0.876	4	HT	–
268	3425851	10.56	2038 \pm 60	92.6 \pm 1.5	1.125	10	SC	9.5 \pm 0.5	47	0.900	2	FT	–
269	7670943	10.93	1895 \pm 73	88.6 \pm 1.3	1.143	19	SC	13.5 \pm 0.6	53	0.827	2	T	–
270	6528464	11.41	1380 \pm 56	75.4 \pm 1.4	1.144	9	SC	3.5 \pm 0.5	34	0.855	2	T	–
271	9451706	11.48	1988 \pm 86	95.0 \pm 1.6	1.067	19	SC	8.1 \pm 0.6	37	0.837	3	T	–
273	3102384	11.46	–	124.3 \pm 1.3	1.026	19	SC	2.4 \pm 0.5	99	0.951	4	HMT	–
274	8077137	11.39	1324 \pm 39	68.80 \pm 0.64	1.186	18	SC	7.7 \pm 0.5	149	0.960	2	HM	–
275	10586004	11.70	1395 \pm 40	69.2 \pm 1.4	1.249	6	SC	3.4 \pm 0.5	37	0.904	2	T	–
276	11133306	11.85	2381 \pm 95	107.9 \pm 1.9	1.033	18	SC	2.8 \pm 0.5	33	0.901	1	T	–
277	11401755	11.87	1250 \pm 44	67.9 \pm 1.2	–	15	SC	–	–	–	–	–	Kepler-36 ^h
279	12314973	11.68	–	78.7 \pm 5.3	1.078	19	SC	15.2 \pm 0.5	27	0.880	1	M	–
280	4141376	11.07	2928 \pm 97	128.8 \pm 1.3	1.037	20	SC	3.5 \pm 0.5	56	0.876	1	T	–
281	4143755	11.95	1458 \pm 57	77.2 \pm 1.3	1.043	18	SC	2.2 \pm 0.6	34	0.836	2	FT	–
282	5088536	11.53	–	109.6 \pm 3.1	1.052	4	SC	3.0 \pm 0.5	28	0.941	1	M	–
285	6196457	11.56	1299 \pm 53	66.6 \pm 1.1	1.118	9	SC	4.2 \pm 0.6	33	0.884	2	MT	–
288	9592705	11.02	1008 \pm 21	53.54 \pm 0.32	1.317	13	SC	9.4 \pm 0.5	41	0.870	3	MT	–
319	8684730	12.71	962 \pm 39	51.7 \pm 1.9	1.201	9	SC	5.9 \pm 0.5	32	0.885	2	T	–
370	8494142	11.93	1133 \pm 81	61.80 \pm 0.76	1.166	15	SC	8.9 \pm 0.5	29	0.835	2	T	–
371	5652983	12.19	–	29.27 \pm 0.36	1.196	15	SC	3.1 \pm 0.6	22	0.866	2	T	–
623	12068975	11.81	2298 \pm 105	108.4 \pm 3.1	1.048	15	SC	2.6 \pm 0.5	33	0.847	3	T	–
674	7277317	13.78	533 \pm 15	33.00 \pm 0.72	1.254	6	SC	1.6 \pm 0.5	54	0.972	1	H	–
974	9414417	9.58	1115 \pm 32	60.05 \pm 0.27	1.636	16	SC	9.3 \pm 0.5	55	0.953	2	T	–
975	3632418	8.22	1153 \pm 32	60.86 \pm 0.55	–	1	SC	–	–	–	–	–	Kepler-21 ⁱ
981	8607720	10.73	159.0 \pm 2.4	12.86 \pm 0.06	2.864	31	LC	2.0 \pm 0.5	54	0.964	5	FT	–
1019	8179973	10.27	341.8 \pm 6.4	22.93 \pm 0.13	4.575	16	SC	2.2 \pm 0.5	93	0.979	4	HMT	–
1054	6032981	11.90	35.1 \pm 0.6	–	2.697	31	LC	7.3 \pm 0.5	24	0.881	3	M	–
1221	3640905	11.58	500.7 \pm 7.0	30.63 \pm 0.20	3.201	9	SC	2.5 \pm 0.5	32	0.945	2	T	–
1222	4060815	12.20	333 \pm 11	22.33 \pm 0.56	4.676	1	SC	2.6 \pm 0.5	25	0.923	2	T	–
1230	6470149	12.26	118.2 \pm 3.7	9.59 \pm 0.04	1.591	31	LC	3.3 \pm 0.5	22	0.903	1	T	–
1241	6448890	12.44	244.3 \pm 3.4	17.40 \pm 0.24	–	31	LC	–	–	–	–	–	Kepler-56 ^j
1282	8822366	12.55	–	71.3 \pm 1.9	1.069	9	SC	7.2 \pm 0.5	29	0.873	2	T	–
1299	10864656	12.18	259.5 \pm 4.3	18.53 \pm 0.17	3.696	9	SC	2.7 \pm 0.5	32	0.940	10	FT	–
1314	10585852	13.24	352.1 \pm 6.9	23.42 \pm 0.23	1.868	9	SC	2.2 \pm 0.5	25	0.935	2	MT	–
1537	9872292	11.74	–	63.8 \pm 1.2	1.135	9	SC	9.6 \pm 0.7	23	0.810	2	M	–

1612	10963065	8.77	2193 ± 48	103.20 ± 0.63	1.571	16	SC	3.4 ± 0.5	180	0.990	4	HT	–
1613	6268648	11.05	–	88.9 ± 2.0	1.105	3	SC	10.6 ± 0.7	28	0.811	2	T	–
1618	7215603	11.60	–	82.4 ± 1.1	1.107	7	SC	11.7 ± 0.5	28	0.871	2	T	–
1621	5561278	11.86	1023 ± 36	56.2 ± 1.7	1.177	6	SC	6.4 ± 0.5	39	0.936	1	T	–
1890	7449136	11.70	–	76.4 ± 1.4	1.104	4	SC	7.8 ± 0.5	41	0.936	2	FM	–
1894	11673802	13.43	–	21.76 ± 0.38	1.338	31	LC	2.8 ± 0.5	22	0.942	1	T	–
1924	5108214	7.84	703 ± 35	41.34 ± 0.67	3.125	3	SC	4.8 ± 0.5	187	0.990	6	FHM	–
1925	9955598	9.44	3546 ± 119	153.18 ± 0.14	1.058	22	SC	1.6 ± 0.5	208	0.985	4	FH	–
1930	5511081	12.12	–	63.3 ± 3.4	1.121	3	SC	4.3 ± 0.5	32	0.932	2	FM	–
1962	5513648	10.77	–	78.6 ± 3.7	1.106	3	SC	3.9 ± 0.5	41	0.926	3	FMT	–
2133	8219268	12.49	108.9 ± 3.0	9.39 ± 0.22	5.393	31	LC	3.2 ± 0.5	21	0.918	3	T	–
2481	4476423	13.61	51.2 ± 1.6	5.09 ± 0.12	4.626	13	LC	5.9 ± 1.3	13	0.707	1	M	–
2545	9696358	11.75	–	51.4 ± 3.7	1.388	1	SC	8.9 ± 0.5	29	0.941	1	M	–
2640	9088780	13.23	76.7 ± 1.3	7.46 ± 0.09	5.433	16	LC	2.0 ± 0.5	56	0.981	1	H	–

The solar reference values for the asteroseismic observations are $\nu_{\max, \odot} = 3090 \pm 30 \mu\text{Hz}$ and $\Delta\nu_{\odot} = 135.1 \pm 0.1 \mu\text{Hz}$ (Huber et al. 2011). “HBR” denotes the height-to-background ratio of the power excess (a measure of signal-to-noise, see e.g. Kallinger et al. 2010a), “Cad” the type of *Kepler* data used for the detection (SC = short-cadence, LC = long-cadence), and “M” the number of months of *Kepler* data used for the analysis. For spectroscopic observations, “CCF” denotes the cross-correlation function (a measure of the quality of the fit compared to the spectral template, see Buchhave et al. 2012), “Sp” the number of spectra used in the analysis, and “Obs” the spectrographs used for the observations (F = FIES, H = HIRES, M = McDonald, T = TRES). References to solutions published in separate papers: a - Barclay et al. (2012), b - Christensen-Dalsgaard et al. (2010), c - Batalha et al. (2011), d - Chaplin et al. (2013), e - Borucki et al. (2012), f - Barclay et al. (2013), g - Gilliland et al. (2013), h - Carter et al. (2012), i - Howell et al. (2012), j - Huber et al. (2013). Note that stars with solutions published in separate papers were not re-analyzed in this study, and hence the columns “HBR” as well as spectroscopic information are not available for these host stars.

TABLE 2 Fundamental Properties of 77 *Kepler* Planet-Candidate Hosts.

KOI	KIC	T_{eff} (K)	[Fe/H]	ρ (g cm^{-3})	$R(R_{\odot})$	$M(M_{\odot})$	Notes
1	11446443	5850 ± 50	−0.15 ± 0.10	1.530 ± 0.030	0.950 ± 0.020	0.940 ± 0.050	Kepler-1 ^a
2	10666592	6350 ± 80	+0.26 ± 0.08	0.2712 ± 0.0032	1.991 ± 0.018	1.520 ± 0.036	Kepler-2 ^b
5	8554498	5753 ± 75	+0.05 ± 0.10	0.2965 ± 0.0092	1.747 ± 0.042	1.130 ± 0.065	–
7	11853905	5781 ± 76	+0.09 ± 0.10	0.427 ± 0.013	1.533 ± 0.040	1.092 ± 0.073	Kepler-4
41	6521045	5825 ± 75	+0.02 ± 0.10	0.457 ± 0.013	1.490 ± 0.035	1.080 ± 0.063	–
42	8866102	6325 ± 75	+0.01 ± 0.10	0.6892 ± 0.0088	1.361 ± 0.018	1.242 ± 0.045	–
64	7051180	5302 ± 75	−0.00 ± 0.10	0.1238 ± 0.0033	2.437 ± 0.072	1.262 ± 0.089	–
69	3544595	5669 ± 75	−0.18 ± 0.10	1.640 ± 0.010	0.921 ± 0.020	0.909 ± 0.057	–
72	11904151	5627 ± 44	−0.15 ± 0.04	1.0680 ± 0.0080	1.056 ± 0.021	0.895 ± 0.060	Kepler-10 ^c
75	7199397	5896 ± 75	−0.17 ± 0.10	0.1152 ± 0.0040	2.527 ± 0.059	1.330 ± 0.069	–
85	5866724	6169 ± 50	+0.09 ± 0.08	0.621 ± 0.011	1.424 ± 0.024	1.273 ± 0.061	Kepler-50 ^d
87	10593626	5642 ± 50	−0.27 ± 0.08	1.458 ± 0.030	0.979 ± 0.020	0.970 ± 0.060	Kepler-22 ^e
97	5780885	6027 ± 75	+0.10 ± 0.10	0.245 ± 0.015	1.962 ± 0.066	1.318 ± 0.089	–
98	10264660	6378 ± 75	−0.02 ± 0.10	0.224 ± 0.014	2.075 ± 0.070	1.391 ± 0.098	Kepler-14
107	11250587	5862 ± 97	+0.27 ± 0.11	0.427 ± 0.032	1.586 ± 0.061	1.201 ± 0.091	–
108	4914423	5845 ± 88	+0.07 ± 0.11	0.513 ± 0.020	1.436 ± 0.039	1.094 ± 0.068	–
113	2306756	5543 ± 79	+0.44 ± 0.10	0.382 ± 0.024	1.580 ± 0.064	1.103 ± 0.097	–
117	10875245	5851 ± 75	+0.27 ± 0.10	0.581 ± 0.049	1.411 ± 0.047	1.142 ± 0.068	–
118	3531558	5747 ± 85	+0.03 ± 0.10	0.581 ± 0.030	1.357 ± 0.040	1.023 ± 0.070	–
119	9471974	5854 ± 92	+0.31 ± 0.11	0.188 ± 0.024	2.192 ± 0.121	1.377 ± 0.089	–
122	8349582	5699 ± 74	+0.30 ± 0.10	0.540 ± 0.019	1.415 ± 0.039	1.084 ± 0.076	–
123	5094751	5952 ± 75	−0.08 ± 0.10	0.641 ± 0.032	1.323 ± 0.037	1.039 ± 0.065	–
168	11512246	5828 ± 100	−0.05 ± 0.10	0.410 ± 0.023	1.548 ± 0.048	1.078 ± 0.077	Kepler-23
244	4349452	6270 ± 79	−0.04 ± 0.10	0.7453 ± 0.0086	1.309 ± 0.023	1.187 ± 0.060	Kepler-25
245	8478994	5417 ± 75	−0.32 ± 0.07	2.458 ± 0.046	0.772 ± 0.026	0.803 ± 0.068	Kepler-37 ^f
246	11295426	5793 ± 74	+0.12 ± 0.07	0.7903 ± 0.0054	1.243 ± 0.019	1.079 ± 0.051	Kepler-68 ^g
257	5514383	6184 ± 81	+0.12 ± 0.10	0.990 ± 0.034	1.188 ± 0.022	1.180 ± 0.053	–
260	8292840	6239 ± 94	−0.14 ± 0.10	0.6652 ± 0.0050	1.358 ± 0.024	1.188 ± 0.059	–
262	11807274	6225 ± 75	−0.00 ± 0.08	0.4410 ± 0.0040	1.584 ± 0.031	1.259 ± 0.072	Kepler-65 ^d
263	10514430	5784 ± 98	−0.11 ± 0.11	0.378 ± 0.011	1.574 ± 0.039	1.045 ± 0.064	–
268	3425851	6343 ± 85	−0.04 ± 0.10	0.662 ± 0.021	1.366 ± 0.026	1.230 ± 0.058	–
269	7670943	6463 ± 110	+0.09 ± 0.11	0.605 ± 0.018	1.447 ± 0.026	1.318 ± 0.057	–
270	6528464	5588 ± 99	−0.10 ± 0.10	0.439 ± 0.016	1.467 ± 0.033	0.969 ± 0.053	–
271	9451706	6106 ± 106	+0.33 ± 0.10	0.697 ± 0.023	1.359 ± 0.035	1.240 ± 0.086	–
273	3102384	5739 ± 75	+0.35 ± 0.10	1.193 ± 0.025	1.081 ± 0.019	1.069 ± 0.048	–
274	8077137	6072 ± 75	−0.09 ± 0.10	0.3653 ± 0.0068	1.659 ± 0.038	1.184 ± 0.074	–
275	10586004	5770 ± 83	+0.29 ± 0.10	0.370 ± 0.015	1.641 ± 0.051	1.197 ± 0.094	–
276	11133306	5982 ± 82	−0.02 ± 0.10	0.898 ± 0.032	1.185 ± 0.026	1.076 ± 0.061	–
277	11401755	5911 ± 66	−0.20 ± 0.06	0.3508 ± 0.0056	1.626 ± 0.019	1.071 ± 0.043	Kepler-36 ^h
279	12314973	6215 ± 89	+0.28 ± 0.10	0.478 ± 0.064	1.570 ± 0.085	1.346 ± 0.084	–

280	4141376	6134 ± 91	-0.24 ± 0.10	1.281 ± 0.027	1.042 ± 0.026	1.032 ± 0.070	-
281	4143755	5622 ± 106	-0.40 ± 0.11	0.459 ± 0.015	1.406 ± 0.041	0.884 ± 0.066	-
282	5088536	5884 ± 75	-0.22 ± 0.10	0.927 ± 0.053	1.127 ± 0.033	0.934 ± 0.059	-
285	6196457	5871 ± 94	+0.17 ± 0.11	0.342 ± 0.011	1.703 ± 0.048	1.207 ± 0.084	-
288	9592705	6174 ± 92	+0.22 ± 0.10	0.2212 ± 0.0027	2.114 ± 0.042	1.490 ± 0.082	-
319	8684730	5882 ± 87	+0.16 ± 0.10	0.206 ± 0.015	2.064 ± 0.076	1.325 ± 0.096	-
370	8494142	6144 ± 106	+0.13 ± 0.10	0.2948 ± 0.0072	1.850 ± 0.050	1.319 ± 0.101	-
371	5652983	5198 ± 95	+0.19 ± 0.11	0.0661 ± 0.0016	3.207 ± 0.107	1.552 ± 0.154	-
623	12068975	6004 ± 102	-0.38 ± 0.10	0.907 ± 0.052	1.120 ± 0.033	0.922 ± 0.059	-
674	7277317	4883 ± 75	+0.16 ± 0.10	0.0840 ± 0.0037	2.690 ± 0.114	1.150 ± 0.120	-
974	9414417	6253 ± 75	-0.13 ± 0.10	0.2783 ± 0.0025	1.851 ± 0.044	1.270 ± 0.086	-
975	3632418	6131 ± 44	-0.15 ± 0.06	0.2886 ± 0.0087	1.860 ± 0.020	1.340 ± 0.010	Kepler-21 ⁱ
981	8607720	5066 ± 75	-0.33 ± 0.10	0.01275 ± 0.00011	5.324 ± 0.107	1.372 ± 0.073	-
1019	8179973	5009 ± 75	-0.02 ± 0.10	0.04057 ± 0.00047	3.585 ± 0.090	1.327 ± 0.094	-
1054*	6032981	5254 ± 97	-0.94 ± 0.16	-	-	-	-
1221	3640905	4991 ± 75	+0.28 ± 0.10	0.07240 ± 0.00094	2.935 ± 0.066	1.298 ± 0.076	-
1222	4060815	5055 ± 75	-0.07 ± 0.10	0.0385 ± 0.0019	3.733 ± 0.176	1.429 ± 0.162	-
1230	6470149	5015 ± 97	-0.21 ± 0.16	0.007091 ± 0.000067	7.062 ± 0.258	1.782 ± 0.193	-
1241	6448890	4840 ± 97	+0.20 ± 0.16	0.02460 ± 0.00060	4.230 ± 0.150	1.320 ± 0.130	Kepler-56 ^j
1282	8822366	6034 ± 92	-0.14 ± 0.10	0.392 ± 0.021	1.592 ± 0.050	1.120 ± 0.083	-
1299	10864656	4995 ± 78	-0.07 ± 0.10	0.02650 ± 0.00049	4.160 ± 0.120	1.353 ± 0.101	-
1314	10585852	5048 ± 75	-0.03 ± 0.10	0.04233 ± 0.00082	3.549 ± 0.104	1.345 ± 0.102	-
1537	9872292	6260 ± 116	+0.10 ± 0.11	0.314 ± 0.011	1.824 ± 0.049	1.366 ± 0.101	-
1612	10963065	6104 ± 74	-0.20 ± 0.10	0.822 ± 0.010	1.225 ± 0.027	1.079 ± 0.069	-
1613	6268648	6044 ± 117	-0.24 ± 0.11	0.609 ± 0.028	1.327 ± 0.041	1.008 ± 0.080	-
1618	7215603	6173 ± 93	+0.17 ± 0.10	0.524 ± 0.013	1.506 ± 0.035	1.270 ± 0.082	-
1621	5561278	6081 ± 75	-0.03 ± 0.10	0.244 ± 0.014	1.954 ± 0.064	1.294 ± 0.093	-
1890	7449136	6099 ± 75	+0.04 ± 0.10	0.450 ± 0.017	1.557 ± 0.040	1.206 ± 0.083	-
1894	11673802	4992 ± 75	+0.04 ± 0.10	0.0365 ± 0.0013	3.790 ± 0.190	1.410 ± 0.214	-
1924	5108214	5844 ± 75	+0.21 ± 0.10	0.1319 ± 0.0043	2.490 ± 0.055	1.443 ± 0.080	-
1925	9955598	5460 ± 75	+0.08 ± 0.10	1.8106 ± 0.0032	0.893 ± 0.018	0.918 ± 0.057	-
1930	5511081	5923 ± 77	-0.07 ± 0.10	0.309 ± 0.034	1.735 ± 0.082	1.142 ± 0.084	-
1962	5513648	5904 ± 85	-0.07 ± 0.10	0.477 ± 0.045	1.470 ± 0.060	1.083 ± 0.071	-
2133	8219268	4605 ± 97	+0.29 ± 0.16	0.00681 ± 0.00032	6.528 ± 0.352	1.344 ± 0.169	-
2481	4476423	4553 ± 97	+0.42 ± 0.16	0.001999 ± 0.000096	10.472 ± 0.696	1.616 ± 0.256	-
2545	9696358	6131 ± 75	+0.13 ± 0.10	0.204 ± 0.029	2.134 ± 0.134	1.417 ± 0.093	-
2640	9088780	4854 ± 97	-0.33 ± 0.16	0.00429 ± 0.00010	7.478 ± 0.246	1.274 ± 0.110	-

Note that ρ is derived directly from scaling relations, while R_{\odot} and M_{\odot} are modeled values using asteroseismic constraints. For references to solutions published in separate papers, see Table 1.

* No full solution was derived for KOI-1054 due to the lack of a reliable $\Delta\nu$ measurement. The asteroseismic surface gravity constrained using ν_{\max} is $\log g = 2.47 \pm 0.01$ dex.

TABLE 3 Re-derived Properties of 107 Planet Candidates in the Sample.

KOI	P (d)	R_p/R_*	$R_p(R_{\oplus})$	a (AU)	$F(F_{\oplus})$
1.01	2.470613200 ± 0.000000100	0.124320 ± 0.000080	12.89 ± 0.27	0.03504 ± 0.00062	773
2.01	2.204735400 ± 0.000000100	0.075450 ± 0.000020	16.39 ± 0.15	0.03812 ± 0.00030	3983
5.01	4.7803287 ± 0.0000030	0.03651 ± 0.00026	6.96 ± 0.17	0.0579 ± 0.0011	897
5.02	7.05186 ± 0.00028	0.00428 ± 0.00038	0.816 ± 0.075	0.0750 ± 0.0014	534
7.01	3.2136641 ± 0.0000042	0.026920 ± 0.000070	4.50 ± 0.12	0.04389 ± 0.00098	1223
41.01	12.815735 ± 0.000053	0.015440 ± 0.000100	2.511 ± 0.062	0.1100 ± 0.0021	190
41.02	6.887099 ± 0.000062	0.00918 ± 0.00016	1.493 ± 0.044	0.0727 ± 0.0014	434
41.03	35.33314 ± 0.00063	0.01042 ± 0.00030	1.694 ± 0.063	0.2162 ± 0.0042	49
42.01	17.834381 ± 0.000031	0.018250 ± 0.000100	2.710 ± 0.039	0.1436 ± 0.0017	129
64.01	1.9510914 ± 0.0000040	0.04015 ± 0.00093	10.68 ± 0.40	0.03302 ± 0.00078	3864
69.01	4.7267482 ± 0.0000052	0.01575 ± 0.00011	1.583 ± 0.037	0.0534 ± 0.0011	276
72.01	0.8374903 ± 0.0000015	0.012650 ± 0.000070	1.458 ± 0.030	0.01676 ± 0.00037	3574
72.02	45.29404 ± 0.00020	0.02014 ± 0.00013	2.321 ± 0.049	0.2397 ± 0.0054	17
75.01	105.88531 ± 0.00033	0.039310 ± 0.000080	10.84 ± 0.25	0.4817 ± 0.0083	30
85.01	5.859933 ± 0.000011	0.018040 ± 0.000080	2.803 ± 0.049	0.0689 ± 0.0011	555
85.02	2.1549189 ± 0.0000083	0.009710 ± 0.000090	1.509 ± 0.029	0.03539 ± 0.00057	2106
85.03	8.131146 ± 0.000051	0.01081 ± 0.00014	1.680 ± 0.036	0.0858 ± 0.0014	358
87.01	289.8622 ± 0.0018	0.0226 ± 0.0016	2.42 ± 0.18	0.849 ± 0.017	1.2
97.01	4.88548920 ± 0.00000090	0.082840 ± 0.000030	17.74 ± 0.59	0.0618 ± 0.0014	1195
98.01	6.7901235 ± 0.0000036	0.056080 ± 0.000050	12.70 ± 0.43	0.0783 ± 0.0018	1042
107.01	7.256999 ± 0.000019	0.02228 ± 0.00011	3.86 ± 0.15	0.0780 ± 0.0020	438
108.01	15.965349 ± 0.000047	0.02224 ± 0.00014	3.484 ± 0.096	0.1279 ± 0.0027	132

108.02	179.6010 ± 0.0012	0.03371 ± 0.00017	5.28 ± 0.14	0.642 ± 0.013	5.2
117.01	14.749102 ± 0.000076	0.02271 ± 0.00016	3.50 ± 0.12	0.1230 ± 0.0025	139
117.02	4.901467 ± 0.000039	0.01321 ± 0.00020	2.034 ± 0.074	0.0590 ± 0.0012	602
117.03	3.179962 ± 0.000025	0.01222 ± 0.00019	1.882 ± 0.069	0.04423 ± 0.00088	1071
117.04	7.95792 ± 0.00017	0.00833 ± 0.00038	1.283 ± 0.072	0.0815 ± 0.0016	315
118.01	24.99334 ± 0.00019	0.01656 ± 0.00024	2.453 ± 0.080	0.1686 ± 0.0039	64
119.01	49.18431 ± 0.00013	0.037540 ± 0.000090	8.98 ± 0.50	0.2923 ± 0.0063	59
119.02	190.3134 ± 0.0020	0.03297 ± 0.00020	7.89 ± 0.44	0.720 ± 0.016	9.8
122.01	11.523063 ± 0.000028	0.02342 ± 0.00020	3.62 ± 0.10	0.1026 ± 0.0024	180
123.01	6.481674 ± 0.000018	0.01686 ± 0.00015	2.434 ± 0.071	0.0689 ± 0.0014	415
123.02	21.222534 ± 0.000093	0.01734 ± 0.00016	2.503 ± 0.073	0.1520 ± 0.0032	85
168.01	10.742491 ± 0.000063	0.02049 ± 0.00018	3.46 ± 0.11	0.0977 ± 0.0023	260
168.02	15.27448 ± 0.00019	0.01376 ± 0.00029	2.325 ± 0.088	0.1235 ± 0.0029	163
168.03	7.10690 ± 0.00012	0.01111 ± 0.00033	1.877 ± 0.081	0.0742 ± 0.0018	451
244.01	12.7203650 ± 0.0000070	0.03583 ± 0.00017	5.117 ± 0.095	0.1129 ± 0.0019	186
244.02	6.2385593 ± 0.0000075	0.018690 ± 0.000090	2.669 ± 0.050	0.0702 ± 0.0012	482
245.01	39.792196 ± 0.000052	0.02513 ± 0.00033	2.117 ± 0.077	0.2120 ± 0.0060	10
245.02	21.30185 ± 0.00013	0.00949 ± 0.00017	0.799 ± 0.030	0.1398 ± 0.0039	24
245.03	13.36726 ± 0.00031	0.00422 ± 0.00027	0.356 ± 0.026	0.1025 ± 0.0029	44
246.01	5.3987665 ± 0.0000071	0.018690 ± 0.000080	2.535 ± 0.040	0.06178 ± 0.00097	409
257.01	6.883403 ± 0.000012	0.02052 ± 0.00015	2.661 ± 0.054	0.0748 ± 0.0011	331
260.01	10.495678 ± 0.000075	0.01125 ± 0.00015	1.667 ± 0.037	0.0994 ± 0.0017	254
260.02	100.28319 ± 0.00085	0.01925 ± 0.00016	2.852 ± 0.057	0.4474 ± 0.0074	13
262.01	7.812512 ± 0.000052	0.01074 ± 0.00015	1.856 ± 0.045	0.0832 ± 0.0016	489
262.02	9.376137 ± 0.000056	0.01362 ± 0.00030	2.354 ± 0.069	0.0940 ± 0.0018	383
263.01	20.71936 ± 0.00019	0.01315 ± 0.00034	2.259 ± 0.081	0.1498 ± 0.0031	111
268.01	110.37908 ± 0.00084	0.02011 ± 0.00015	2.997 ± 0.061	0.4826 ± 0.0076	12
269.01	18.01134 ± 0.00022	0.01074 ± 0.00019	1.696 ± 0.043	0.1475 ± 0.0021	151
270.01	12.58250 ± 0.00014	0.01127 ± 0.00020	1.804 ± 0.052	0.1048 ± 0.0019	172
270.02	33.67312 ± 0.00049	0.01334 ± 0.00024	2.135 ± 0.062	0.2020 ± 0.0037	46
271.01	48.63070 ± 0.00041	0.01876 ± 0.00021	2.782 ± 0.078	0.2801 ± 0.0065	29
271.02	29.39234 ± 0.00018	0.01785 ± 0.00016	2.647 ± 0.072	0.2003 ± 0.0046	57
273.01	10.573769 ± 0.000026	0.0156 ± 0.00029	1.84 ± 0.35	0.0964 ± 0.0015	122
274.01	15.09205 ± 0.00035	0.00663 ± 0.00033	1.200 ± 0.066	0.1264 ± 0.0026	210
274.02	22.79519 ± 0.00063	0.00667 ± 0.00036	1.208 ± 0.071	0.1665 ± 0.0035	121
275.01	15.79186 ± 0.00014	0.01316 ± 0.00015	2.357 ± 0.078	0.1308 ± 0.0034	157
275.02	82.1997 ± 0.0020	0.01375 ± 0.00032	2.463 ± 0.096	0.393 ± 0.010	17
276.01	41.74591 ± 0.00018	0.02052 ± 0.00082	2.65 ± 0.12	0.2413 ± 0.0045	28
277.01	16.231204 ± 0.000054	0.021810 ± 0.000100	3.870 ± 0.049	0.1284 ± 0.0017	176
279.01	28.455113 ± 0.000053	0.0351 ± 0.00015	6.01 ± 0.41	0.2014 ± 0.0042	81
279.02	15.41298 ± 0.00012	0.0158 ± 0.00034	2.72 ± 0.60	0.1338 ± 0.0028	184
280.01	11.872914 ± 0.000023	0.01972 ± 0.00073	2.242 ± 0.100	0.1029 ± 0.0023	130
281.01	19.55663 ± 0.00011	0.01689 ± 0.00012	2.592 ± 0.078	0.1363 ± 0.0034	95
282.01	27.508733 ± 0.000086	0.02774 ± 0.00013	3.41 ± 0.10	0.1743 ± 0.0037	45
282.02	8.457489 ± 0.000097	0.00969 ± 0.00028	1.191 ± 0.049	0.0794 ± 0.0017	217
285.01	13.748761 ± 0.000072	0.02026 ± 0.00017	3.77 ± 0.11	0.1196 ± 0.0028	216
288.01	10.275394 ± 0.000058	0.01463 ± 0.00013	3.376 ± 0.073	0.1057 ± 0.0019	522
319.01	46.15159 ± 0.00011	0.04655 ± 0.00024	10.49 ± 0.39	0.2765 ± 0.0067	60
370.01	42.88255 ± 0.00031	0.01998 ± 0.00015	4.03 ± 0.11	0.2630 ± 0.0067	63
370.02	22.95036 ± 0.00032	0.01227 ± 0.00034	2.477 ± 0.096	0.1733 ± 0.0044	146
623.01	10.34971 ± 0.00012	0.01062 ± 0.00027	1.298 ± 0.050	0.0905 ± 0.0019	179
623.02	15.67749 ± 0.00020	0.01106 ± 0.00026	1.351 ± 0.051	0.1193 ± 0.0026	103
623.03	5.599359 ± 0.000062	0.00918 ± 0.00023	1.122 ± 0.043	0.0601 ± 0.0013	405
674.01	16.338952 ± 0.000071	0.04259 ± 0.00022	12.50 ± 0.54	0.1320 ± 0.0046	212
974.01	53.50607 ± 0.00061	0.01353 ± 0.00014	2.733 ± 0.071	0.3010 ± 0.0068	52
975.01	2.785819 ± 0.000017	0.007740 ± 0.000100	1.571 ± 0.026	0.04272 ± 0.00011	2405
981.01	3.99780 ± 0.00012	0.00819 ± 0.00053	4.76 ± 0.32	0.05478 ± 0.00098	5586
1019.01*	2.497052 ± 0.000063	0.00689 ± 0.00041	2.70 ± 0.17	0.03958 ± 0.00094	4637
1221.01	30.16012 ± 0.00052	0.01469 ± 0.00034	4.71 ± 0.15	0.2069 ± 0.0040	112
1221.02	51.0802 ± 0.0018	0.01106 ± 0.00039	3.54 ± 0.15	0.2939 ± 0.0057	56
1222.01	4.28553 ± 0.00014	0.00649 ± 0.00065	2.64 ± 0.29	0.0582 ± 0.0022	2416
1230.01 ⁺	165.72106 ± 0.00077	0.08259 ± 0.00018	63.64 ± 2.33	0.716 ± 0.026	55
1241.01	21.40505 ± 0.00036	0.02292 ± 0.00033	10.58 ± 0.40	0.1655 ± 0.0054	322
1241.02	10.50343 ± 0.00025	0.01120 ± 0.00033	5.17 ± 0.24	0.1030 ± 0.0034	832
1282.01	30.86392 ± 0.00031	0.01428 ± 0.00018	2.480 ± 0.084	0.2000 ± 0.0049	75
1299.01	52.50128 ± 0.00067	0.02683 ± 0.00030	12.18 ± 0.38	0.3035 ± 0.0076	105
1314.01	8.57507 ± 0.00018	0.01191 ± 0.00027	4.61 ± 0.17	0.0905 ± 0.0023	896
1537.01	10.19144 ± 0.00022	0.00675 ± 0.00020	1.343 ± 0.054	0.1021 ± 0.0025	440

1612.01	2.464999 ± 0.000020	0.00531 ± 0.00025	0.710 ± 0.037	0.03663 ± 0.00078	1394
1613.01	15.86621 ± 0.00020	0.00933 ± 0.00064	1.35 ± 0.10	0.1239 ± 0.0033	137
1618.01	2.364320 ± 0.000036	0.00547 ± 0.00020	0.899 ± 0.039	0.03761 ± 0.00081	2089
1621.01	20.31035 ± 0.00024	0.01290 ± 0.00027	2.75 ± 0.11	0.1588 ± 0.0038	186
1890.01	4.336491 ± 0.000029	0.01035 ± 0.00014	1.758 ± 0.051	0.0554 ± 0.0013	981
1894.01	5.288016 ± 0.000045	0.01733 ± 0.00019	7.17 ± 0.37	0.0666 ± 0.0034	1805
1924.01*	2.119128 ± 0.000038	0.00645 ± 0.00022	1.753 ± 0.071	0.03649 ± 0.00067	4878
1925.01	68.95800 ± 0.00090	0.0108 ± 0.0038	1.05 ± 0.37	0.3199 ± 0.0066	6.2
1930.01	13.72686 ± 0.00014	0.01341 ± 0.00020	2.54 ± 0.13	0.1173 ± 0.0029	242
1930.02	24.31058 ± 0.00036	0.01298 ± 0.00026	2.46 ± 0.13	0.1717 ± 0.0042	113
1930.03	44.43150 ± 0.00076	0.01492 ± 0.00027	2.83 ± 0.14	0.2566 ± 0.0063	51
1930.04	9.34131 ± 0.00021	0.00824 ± 0.00032	1.560 ± 0.096	0.0907 ± 0.0022	404
1962.01	32.85833 ± 0.00033	0.01593 ± 0.00058	2.55 ± 0.14	0.2062 ± 0.0045	55
2133.01	6.246580 ± 0.000082	0.01798 ± 0.00026	12.81 ± 0.72	0.0733 ± 0.0031	3205
2481.01 ⁺	33.84760 ± 0.00091	0.02750 ± 0.00072	31.42 ± 2.24	0.240 ± 0.013	733
2545.01	6.98158 ± 0.00019	0.00568 ± 0.00025	1.32 ± 0.10	0.0803 ± 0.0018	896
2640.01	33.1809 ± 0.0014	0.02086 ± 0.00072	17.02 ± 0.81	0.2191 ± 0.0063	581

Planet period and planet-star size ratio have been adopted from Batalha et al. (2013). The incident flux $F(F_{\oplus})$ has been estimated using the planet-star separation given in Batalha et al. (2013) and assuming circular orbits ($d/R_* = a/R_*$). Note that KOI-113.01, KOI-245.04, KOI-371.01 and KOI-1054.01 have been omitted either due to large uncertainties in the transit parameters given in Batalha et al. (2013) or due to evidence that the transit events are false-positives.

⁺ Asteroseismic false-positive.

* Low-mass stellar companion detected by follow-up radial-velocity observations.